Soft Matter

Accepted Manuscript

ROYAL SOCIETY OF CHEMISTRY

www.rsc.org/softmatter

Instability, Self Organization and Pattern Formation in Thin Soft Films

Rabibrata Mukherjee[1¶] and Ashutosh Sharma[2]*

[1]Instability and Soft Patterning Laboratory, Department of Chemical Engineering, Indian Institute of Technology Kharagpur, 721 302, India

[2]Department of Chemical Engineering and Nano-science Center, Indian Institute of Technology Kanpur, 208016, India

Abstract:

The free surface of a thin soft polymer film is often seen to become unstable and self-organizes in into various meso scale structures such as holes, droplets, ribbons, pillars, bi-continuous labyrinths etc. Such patterns, though inherently isotropic usually exhibit well-defined mean length-scales and feature sizes governed by interplay of destabilizing inter-surface interactions, surface tension and viscoelasticity. In this article we classify instability of a thin polymer film into three broad categories, which are: Category 1: Instability of an ultra-thin (< 100 nm) viscous film engendered by amplification of thermally excited surface capillary waves due to interfacial dispersive van der Waals forces; Category 2: instability arising from the attractive inter-surface interactions between the free surface of a soft film exhibiting room temperature elasticity and another rigid surface in its contact proximity; and Category 3: instability caused by an externally applied field such as electric field or thermal gradient, observed in both viscous and elastic films. We review the salient features of each instability class and highlight how characteristic length scale, feature morphology, evolution pathway, etc. depends on initial properties such as film thickness, visco-elasticity (rheology), residual stress, film preparation conditions etc. We emphasize various possible strategies for aligning and ordering of the otherwise isotropic structures by combining the essential concepts of bottom-up and top-down approaches resulting in self-organization mediated novel micro and nano scale fabrication strategies in soft materials. Basic theoretical concepts associated with each instability setting is briefly discussed for a better understanding of the underlying physics, leading to a unified understanding of these apparently distinct instability classes as the limiting cases of a general framework of instability in a visco-elastic thin film. A perspective including possible future direction of research, novelty and limitations of the methods, particularly in comparison to the existing patterning techniques is also presented for each setting.

¶ rabibrata@che.iitkgp.ernet.in ; * ashutos@iitk.ac.in

1.0 Introduction:

Polymer thin films are ubiquitous in many applications like optoelectronics,[1] biotechnology,[2] nanolithography,[3] sensors and actuators,[4] microfluidics,[5] functional coatings and lubricants.[6] A highly confined thin film is often away from thermodynamic equilibrium and as a result, it evolves to a lower energy configurations by spontaneous morphological transformation from an initially flat film to a micro/nano structured morphology, including possible disintegration of the film.[7] We refer to the shaping of an initially featureless film due to such instabilities, which can be spontaneous or can be mediated by an externally imposed force field as Self organization.[8] This is clearly distinct from the Self-Assembly,[9,10] where a large number of molecules/ small building blocks come together and assemble in an ordered fashion to form a larger supra-molecular assembly. In contrast, Self-Organization involves spontaneous change of shape from a simple to a more complex organization. As an example, a thin film spontaneously fragmenting into an array of holes or droplets due to instability is opposite of the self-assembly, though minimization of the free energy remains the key driving force in both the cases. It thus becomes important to understand the underlying science of thin film instability,[11-27] so that ultra-thin defect free, stable coatings can be engineered in some applications and in others, morphology of the self organized patterns can be controlled to achieve desired surface topography and functionality, particularly in functional coatings that regulate wetting (super-hydrophobic/ oleophobic),[28] adhesion and friction,[29] colors,[30] among many other interfacial properties and interactions.

Initial research on instability and meso-mechanics of soft thin films has mostly evolved along two distinct paths: (a) studies involving a purely viscous liquid thin film, either free or supported on a solid substrate (wetting film), and (b) soft, purely elastic film sandwiched between two rigid

substrates, which is a special case of the adhesive film. If the film is very thin (< 100 nm), excess van der Waals force and other inter-surface interactions can destabilize the film. An externally applied force field such as an electric field or a thermal gradient can also destabilize both types of films. To facilitate discussion, we classify possible instabilities of a thin polymer film into three broad categories based on the nature of the confining field. **Category 1:** Instability in ultra-thin wetting films engendered by interfacial nonpolar van der Waals and other polar interactions, leading to spontaneous rupture and dewetting of viscous and viscoelastic films.[31–295] **Category 2:** instability triggered by inter-surface adhesive interaction between the film and a contacting surface, observed mostly in soft elastic films.[296–352] C**ategory 3:** Instability engendered by an external field such as an electric filed or a thermal gradient, observed in both viscous and elastic films.[353–396] In case of **Category 1** instability, the destabilizing inter-surface interactions decrease rapidly with increase in the film thickness (**h**), and therefore relatively thicker films (**h** > few tens of nm) rupture only by nucleation around physico-chemical defects. Category 1 instability has a long-wave character ($\lambda >> \mathbf{h}$) and its growth is associated with flow of liquid from the thinner to thicker, intact parts of the film.[8,58–148] In contrast, there is no convective material transport in case of contact proximity induced category 2 instability observed in a soft solid film. In this case, elastic deformation of the film surface results in short wave contact instability ($\lambda \approx 3\mathbf{h}$) due to minimization of elastic strain energy.[303–310]

It is well known that in many nonlinear and complex systems, the equilibrium state is often not unique and there can be several metastable states corresponding to local energy minima.[8,58] This particular aspect of freezing the patterns at any intermediate stage allows potential engineering of many distinct structures in the same system, which is a distinct advantage over conventional soft lithography based replication techniques widely used for nano patterning in soft materials. The

possibility of aligning and ordering the intrinsically isotropic instability patterns by a creative combination of the top down and bottom up approaches has also received significant research attention, across all the categories.

In what follows, we present a consolidated and detailed review of various types of instabilities and pattern formation in soft thin films, without any phase change. The review mostly focuses on experimental findings, though the essential theoretical concepts are also included for completeness. The article is organized according to the different categories of instability classes. As several reviews on category 1 instability involving dewetting are already available,[31-47] we discuss this section rather briefly and focus more on categories 2 and 3, which lack extended reviews.

2.0 Category 1 Instability: Spontaneous Rupture and Dewetting of Thin Polymer Films

2.1 Dewetting of thin Liquid Films: Basic Theory and Mechanism

Coating techniques such as spin and dip coating of polymer solutions are commonly used to create a thin polymer film on a solid substrate regardless of its wettability, and this allows obtaining an initially intact, flat film on a non wettable substrate which is thermodynamically unstable. Enhanced chain mobility above glass transition temperature of the constituent polymer allows growth of surface instability leading to increasing deformation and even disintegration of such a film.[49–83] While relatively thicker films (**h** > few hundreds of nm) are stabilized due to gravity, the issue of spontaneous film rupture becomes unavoidable in films thinner than about 100 nm, where the stability is strongly influenced by the integrated intermolecular forces across the film.[73,74,102] The linearized Navier Stokes equation for a non-slipping, isothermal, single component, Newtonian liquid film without evaporation/condensation, incorporating the influence of intermolecular forces and simplified in the lubrication approximation (negligible inertial effects), on a physically or chemically structured substrate exhibiting long wave instability

($\boldsymbol{\lambda}$>>**h**), which captures the dynamics and evolution of a non wettable thin film rather accurately is given as: [72,99,100,109, 238–242]

$$3\mu h_t + [(h - af)^3 \{\gamma(h_{xx} + h_{yy}) - \phi\}_x]_x + [(h - af)^3 \{\gamma(h_{xx} + h_{yy}) - \phi\}_y]_y = 0 \qquad (1)$$

where subscripts denote partial derivatives; $h = h(x,y,t)$ is the local film thickness; ϕ is the effective interface potential per unit volume ($\phi = \partial \Delta G/\partial h$), which is also referred to as the Conjoining Pressure (and $-\phi$ as disjoining pressure), ΔG is excess interaction energy per unit area which depends on the local thickness. The term $z = af(x,y)$ quantifies the physical roughness of the substrate, and a = 0 for a smooth, homogeneous substrate. On a physico-chemically rough (patterned) substrate the functional form of the term ϕ_x based on linearization is:

$$\phi_x = (\partial\phi/\partial h)(\partial h/\partial x) + (\partial\phi/\partial x)|_h \qquad (2)$$

The second term represents the in-plane potential gradient due to substrate non-homogeneity and vanishes on a homogeneous substrate. Equation (1) is extensively used in assessing the stability of an initially uniform film of mean thickness h_0.[72] The stability of a film is tested from this equation by checking the response of the free surface to a periodic small amplitude perturbation ($\varepsilon << h_0$) of wavenumber **k**, of the form:

$$h(x, t) = h_0 + \varepsilon \sin(kx) \exp(\omega t) \qquad (3)$$

where ω is the initial growth coefficient. From linear stability analysis, it is possible to obtain:

$$\omega = C\,[-\gamma k^4 - (\partial\phi/\partial h)k^2] \qquad (4)$$

From equation 3, it can be clearly understood that for the perturbation to grow with time, ω must be positive. This becomes possible only when $\partial\phi/\partial h < 0$, as the first term in equation 4, which represents the effect of surface tension is always negative and therefore has an unconditional stabilizing effect.[72] Thus, a film can be distinguished as *unconditionally stable* or *perfectly wetting* ($\partial\phi/\partial h > 0$ for all **h**); *unstable* ($\partial\phi/\partial h < 0$) and *metastable* ($\partial\phi/\partial h > 0$ only up to certain

specific value of **hc** and $\partial\phi/\partial h<0$ beyond **h>hc**).[62,72,73,99,100,103,109] Metastable films rupture due to finite amplitude thermal fluctuation at the surface or by nucleation around a defect, where the local film thickness is often lower. When $\partial\phi/\partial h<0$, the growth of instability is spontaneous and is referred to as *spinodal dewetting* due to its similarity with the well-known spinodal decomposition in fluid mixtures. The term $\partial\phi/\partial h$ is referred to as the spinodal parameter as it plays the same role as the effective diffusivity in the phase separating mixtures. The variation of ϕ with **h** for a stable, unstable and a metastable film is qualitatively shown in figure 1A.[62,75]

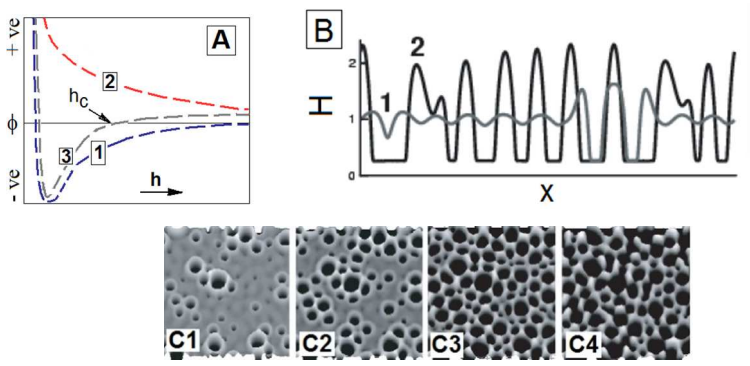

Figure 1: (A) Indicative ϕ vs h. plots for a spinodally unstable (line 1), stable (line 2) and metastable (line 3) film respectively. The metastable film is stable for $h > h_C$ and unstable for $h < h_C$. (B) A typical LSA result showing formation of 9 holes on a 10 λ domain for a 5.5 nm thick film for which h_C = 6.8 nm. (C) Time evolution (c1 → c4) of instability in a 5.5 nm film on a 10λ × 10λ domain, based on non linear simulations starting with a random roughness of 1% maximum amplitude at initial time. The images correspond to τ = 0.933, 0.992, 1.060 and 1.129 respectively, where τ is calculated from eqn. 5C. B and C reproduced with permission from ref. 72. Copyright 2003, European Physical Society.

The wave number at which the growth coefficient is maximized is $\mathbf{K_m} = [(-\partial\phi/\partial h)/2\gamma]^{1/2}$, which can beeasily obtained by setting $\partial\omega/\partial k = 0$.[62] The corresponding wavelength, $\lambda_m = 2\pi/k_m$ represents the short time initial length scale of instability, which often persists to later stages of dewetting as well arguably due to strong pinning, and in experiments, manifest as the mean spacing between holes.[62,72] The corresponding expressions for λ_m, N_m (number density of features) and corresponding linear time scale for destabilization (τ) are:[72]

$$\lambda_m = [-8\pi^2 \gamma /(-\partial\phi/\partial h)]^{1/2} \qquad (5A)$$

$$N_m = \lambda_m^{-2} = -(\partial\phi/\partial h)/ 8\pi^2\gamma \qquad (5B)$$

$$\boldsymbol{\tau} = 12\,\boldsymbol{\gamma\mu}\,[h^3\,(\partial\phi/\partial\mathbf{h})^2]^{-1}\,\ln(\mathbf{h}/\,\boldsymbol{\varepsilon}) \qquad (5C)$$

The above entities can be calculated and directly compared with experimental findings, if a functional form of $\boldsymbol{\phi}$ is available, which for an unsteady film is constituted of antagonistic interactions with different decay characteristics. The two most significant interactions are the long range a-polar van der Waals force and shorter range polar interactions.[72,73,85] It is important to point out that no instability is possible in the absence of an interfacial attraction, as any long range interfacial repulsion would stabilize the film (curve 2, figure 1A). A popular representation of $\boldsymbol{\phi}$ for an unstructured thin liquid film that works rather well for a variety of materials including polymers is:[72]

$$\boldsymbol{\phi} = (\mathbf{A_s}/6\pi\mathbf{h}^3) - (\boldsymbol{S}_P/\boldsymbol{l}_P)\exp(-\boldsymbol{h}/\boldsymbol{l}_P) - (B/\boldsymbol{h}^9) \qquad (6)$$

Where $\mathbf{A_s}$ refers to the effective Hamaker constant for van der Waals interaction; a positive or negative value of $\mathbf{A_s}$ denotes long-range attraction or repulsion, respectively. $\mathbf{S_P}$ denotes the strength of any medium or short- range interaction, which can be attractive ($\mathbf{S_P} < 0$) or repulsive ($\mathbf{S_P} > 0$); $\mathbf{l_P}$ is the corresponding decay length. This term accounts for any acid-base (AB) type interactions in a polar liquid like water (hydrophobic repulsion) as well as the entropic confinement effects due to adsorption/ grafting of polymer brushes at the film–substrate interface. The third Born repulsion term is included in simulations to remove any possible nonphysical singularity at rupture as $\boldsymbol{h} \rightarrow 0$.[70,72]

It can be seen from equation (6) that $\partial\boldsymbol{\phi}/\partial\mathbf{h} = -\mathbf{A_S}/2\pi\mathbf{h}^4$ (considering only the first term). Thus, the van der Waals force is destabilizing when $\mathbf{A_S}$ is positive, signifying an attractive interfacial interaction.[48,58–63,72,82,117] Under such a condition, the attractive interaction grows stronger with a decline in the local thickness and amplification of the thermal fluctuations at the free surface of the film. The growing amplitude eventually leads to the rupture of the film with formation of

holes, which subsequently grow, coalesce with neighboring holes and eventually lead to isolated, random droplets.[62,72,82] This analysis is however valid only for unstable and metastable films ($\mathbf{h} < \mathbf{h_C}$).[72,82] A thermodynamically stable film can also rupture due to nucleation around substrate defects or heterogeneities such as dust, trapped micro-cavities, chemical contamination *etc*. which results in a non zero $(\partial\phi/\partial x)|_h$ term in equation (2) even on a smooth fully wettable surface. If the in-plane potential gradient supplies adequate driving force to the liquid to flow out of the heterogeneous patches, the local $\boldsymbol{h}$ may $\rightarrow$ 0, a scenario that is known as "true" or "heterogeneous" nucleation.[72,73,103,117] The same mechanism can lead to reduction of local film thickness well below $\mathbf{h_C}$ in a metastable film having initial $\mathbf{h} > \mathbf{h_C}$, and thus trigger instability.[111] On the other hand, a metastable film with initial $\mathbf{h}$ just above the spinodal boundary ($\mathbf{h}$ marginally > $\mathbf{h_C}$) can rupture due to "thermal" or "homogeneous" nucleation, as the term $\partial\phi/\partial\mathbf{h}$ might undergo a local reversal in sign due to fluctuations present on the free surface of the film.[72,78] This regime is often referred to as the "defect sensitive spinodal regime" (DSSR),[72] and is clearly distinct from possible nucleated rupture of a film even within the spinodal envelop.[102,103] In case both the modes of instability are co-operative in a specific film, the morphological evolution is governed by the mode with a faster time scale of evolution, though the final morphology often bears the signature of both the modes in experimnets.[72,73]

Initially, nucleation was considered to be the only mechanism possible for the rupture of stable films, which includes thick films and films on wettable substrates. However, many experiments reported dewetting of thicker thermodynamically stable films on wettable substrates, including the classic example of the extremely well investigated dewetting of a polystyrene (PS) thin film on a native oxide coated silicon wafer substrate![31-46,77–79,81–83,89,95,97,102–104,106,107,109,110,113–119,139–143,146–152,157,168,175,177–179,184,186,190–197,199–206,212] Particularly, many experiments that deal with

dewetting of films having thickness in the range of 20 – 80 nm, where the chances of spinodal instability is negligible as the spinodal parameter becomes too weak, still report scaling relations between $\mathbf{N_m}$ and $\boldsymbol{\lambda_m}$ with **h** which follows equations 5A and 5B respectively![43,93,160] Bollinne et al. reported spinodal like dewetting in 15 nm thick PS films, though they found that the temporal dependence of the wavelength of the growing instability did not fully agree with the classical theory of spinodal dewetting.[157] To justify such enigmatic occurrences, as well as to account for observations such as satellite hole formation,[114,115] variation of $\mathbf{N_m}$ as a function of aging time etc.[168] several other mechanisms like localized density variation along the film thickness,[158,159] additional forces arising out of confinement of thermally excited acoustic waves,[160] effect of thermal noise,[161] influence of molecular recoiling,[162] effect of chain ends,[163] choice of solvent during coating,[164] substrate cleaning procedures,[165] etc. have been proposed over the years. Reiter and coworkers have shown that residual stresses generated during spin coating and subsequent film drying play a major role in dewetting in high molecular weight films beyond the chain entanglement limit.[168] Their work show that the probability of hole nucleation reduces with longer aging and annealing, and is manifested as reduced $\mathbf{N_m}$ of holes in samples aged longer (for months).[168]

While linear stability analysis (LSA) is useful for assessing the stability of a film, it does not provide adequate details about the precise shape and evolution sequence of the structures and prescribes a featureless superposition of randomly oriented small amplitude waves, as can be seen in figure 1B.[72] The limitation of LSA has been overcome based on full three-dimensional (3D) nonlinear simulations that predict the morphology of an evolving film during different stages, allowing direct comparison with experiments.[51,63,70,99,114,115] For the simulations, equation (1) in a non-dimensional form is discretized in space. The resultant set of coupled ordinary

differential equations (ODEs) are solved as an initial value problem with a volume preserving initial random perturbation, or other forms of initial perturbations with periodic boundary conditions.[70] A typical set of predicted morphology based on non linear simulations is shown in figure 1C.[70] Complex dewetted morphology as well as dewetting pathway in various settings have been fully captured by 3-D simulations, and favorably compared with experimental findings.[51,70,2,73,113–115]

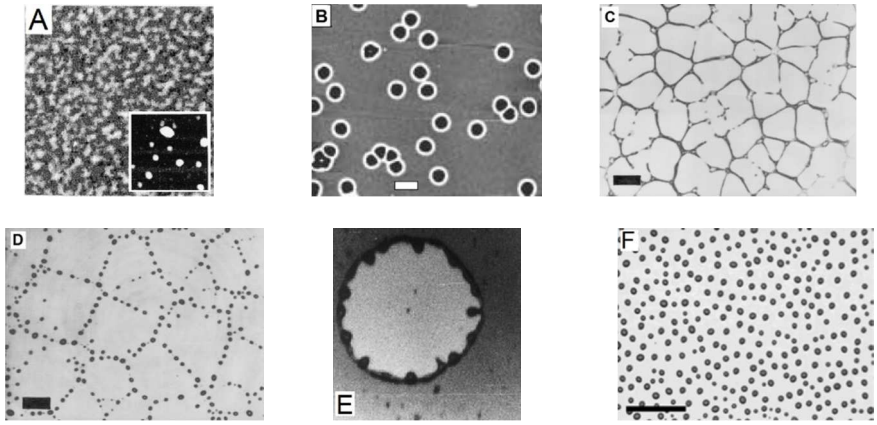

Figure 2: Typical morphologies associated with dewetting of thin polymer films: (A) Undulations in the early stages of dewetting in a 4.5 nm thick PS film annealed at 115 ^{o}C for 4 minutes. Inset shows late stage coarsening into large drops. Reproduced with permission from ref. 83. Copyright 1998 American Physical Society; (B) formation of nucleated holes in a 6.6 nm thick PS film. Reproduced with permission from ref. 102. Copyright 2001 American Physical Society; (C) Polygonal patterns with largely intact rim observed in a 10 nm thick PS film on a silanized silicon wafer (D) Final polygonal pattern formed in a 45 nm thick PS film after decay of rims into spherical droplets due to Rayleigh instability (C, D: Scale bar 70 μm); (E) Signature of fingering instabilities and generation of drops from an expanding hole in a 50-nm-thick polystyrene film. (C, D and E) Reproduced with permission from ref. 82. Copyright 1996 Academic Press; (F) Random collection of polymer droplets resulting from the dewetting of a 24 nm thick PS film on a crosslinked PDMS substrate. There was no polygon formation during dewetting. Reproduced with permission from ref. 90. Copyright 2008, Royal Society of Chemistry.

2.2 Dewetting of Thin Polymer Films: Experiments

Experimentally, dewetting of thin polymer films have been investigated for a wide variety of materials, though dewetting of PS thin films on silicon substrate has received maximum attention, arguably due to easy availability of PS! [31-46,77–79,81–83,89,95,97,102–104,106,107,109,110,113–119,139–143,146–152,157,168,175,177–179,184,186,190–197,199–206,212] Other polymers that have been used for dewetting experiments include poly-methylmethacrylate (PMMA),[144,160] poly-dimethylsiloxane (PDMS),[76,85,87,94,169] perfluoroalkylmethacrylate,[126] perfluoropolyether (PFPE),[85,132]

polyethylenepropylene (PEP),[81] poly(4-vinylpyridine) (P4VP),[126] and in various liquid crystals such as CB5 and CB8.[127–131]

True spinodal dewetting takes place in extremely thin films (**h** < 5 nm) and is therefore difficult to capture, as substrate heterogeneities tend to rupture such films in most cases.[72,73,95,97,101,118] The undulating, bi-continuous features in spinodal dewetting, shown in figure 2A was first captured by Xie et al. in a 4.5 nm thick low molecular weight PS film ($\mathbf{M_W}$ = 4K) on silicon substrate.[83] The average amplitude of the undulations grow with time in spinodal dewetting, and the film eventually disintegrates into small, uniformly sized droplets. These droplets at late stages coarsen through a coalescence process (inset of figure 2A).[83] Similar undulations have subsequently been captured by Herminghuas and Steiner in films of similar thickness.[102,160] Seeman et al. captured clear distinction in the morphology and dewetting pathway between spinodal, homogeneous and heterogeneous dewetting.[102,104]

Experiments with thicker films in many cases carry a combined signature of spinodal and nucleated dewetting.[97,102–104,112–115] where the onset of instability is with the appearance of nearly equal sized, random holes which grow with time (figure 2B). A distinct rim appears around the holes just ahead of the moving contact line due to mismatch in the rates at which the polymer is dislodged from the substrate and redistributed over other intact parts of the film.[76–78,82,89,90,97,102–104,106–115,133–139, 142,144,168,170,171,179–186,192–206] A two stage growth mechanism is observed during hole formation: a slow initial phase till the appearance of holes followed by a faster hole growth exhibiting a power law behavior.[146] Growth of adjacent holes results in coalescence of the rims, forming a network of polymer ribbons known as the cellular pattern (figure 2C), which subsequently break down into isolated droplets,[77,78,82] due to Rayleigh Instability.[215,216] Appearance of satellite holes around the rims of pre-existing holes leading to a hole formation

cascade is often observed in nucleated dewetting.[108,115] Satellite hole formation is favored by the precise profile of the rim, as they are seen to form in locations where the rim has a locally depleted shallow profile towards the intact side of the film.[113] In films of high molecular weight polymers, the rim often exhibits secondary instability in the form of undulating fingers (figure 2E) and eventually disintegrate in to corona of liquid droplets along the inner perimeter of the hole on non wettable substrates, due to Rayleigh–Plateau instability.[90,128,133–139] In such a scenario, the final dewetted morphology comprises of completely random collection of droplets (figure 2F),[90] rather than droplets arranged along the arms of the cellular patterns (figure 2D in absence of rim instability.[77]

Dewetting in a polymer film is typically engendered by heating the film beyond the $\mathbf{T_G}$ of the polymer, which results in significant reduction of viscosity. It is argued that in ultra-confined thin films, there is potential reduction of $\mathbf{T_G}$ as compared to bulk, due to reduced packing density of the polymer molecules, which induce additional mobility to the molecules, and dewetting may take place even at temperatures below the bulk $\mathbf{T_G}$.[121] Exposing the film to its solvent vapor is the other preferred route to initiate dewetting, where the solvent molecules penetrate into the polymer matrix and effectively lower the $\mathbf{T_G}$ below the room temperature. [90,142,144,] Solvent assisted dewetting has been observed during chemical vapor deposition of a polymer thin film.[145] Xu *et al*. have reported a non solvent induced dewetting of PS thin film on a hydrophilic surface at room temperature in the presence of water vapor. The water molecules penetrate to the hydrophilic substrate and dislodge the polymer molecules following a penetration-replacement mechanism.[143]

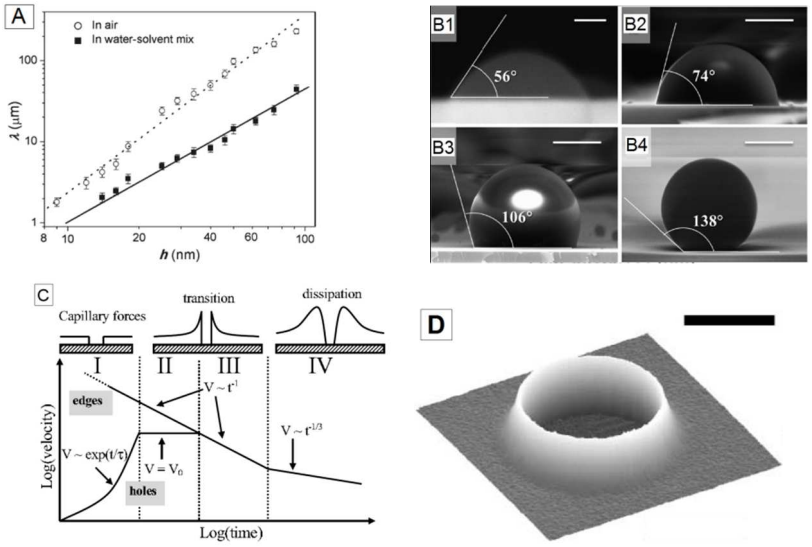

Figure 3: (A) Double-logarithmic plot of wavelength or the mean separation between holes (λ) as a function of PS film thickness for dewetting in air and in water solvent mix. The slope of the best fit line is 1.51 ± 0.06 in case of the water solvent mix as opposed to 2.19 ± 0.07 for air. (B) Time evolution of contact angles of dewetted droplets of a 22 nm PS film showing large contact angles in case of dewetting in water solvent mixture, after : (B1) 3 min, (B2) 10 min, (c) 20 min, and (d) 1 hour. Scale bar: 500 nm. (A,B: reproduced with permission from ref. 150. Copyright 2011, American Chemical Society. (C) Schematic of the overall dewetting behavior of a nonlinear viscoelastic polymer film along with associated rim shapes. reproduced with permission from ref. 186. Copyright 2003, American Physical Society; (D) Anisotropic rim formed due to dewetting of a 24 nm thick visco elastic PS film after annealing at 120^{O}C for 80 minutes. Scale bar is 5 μm. reproduced with permission from ref. 177. Copyright 2001, American Physical Society.

Recently, Verma *et al*. reported a rapid, room temperature dewetting protocol which reduces the instability length scale by more than an order. [149–151] The film is immersed in a mixture of a good solvent and a non-solvent, for example, a mixture of MEK and water for dewetting of PS and PMMA films.[149–151] The good solvent selectively permeates into the film, reducing its $\mathbf{T_G}$ below room temperature and simultaneously lowering the stabilizing interfacial tension to nearly zero. Presence of a large amount of water (non solvent) in the solution prevents complete dissolution of the polymer film. The presence of (polar) water additionally results in a strong destabilizing electrostatic force. A combination of all these leads to extremely fast dewetting and results in much smaller features. In particular, lower interfacial tension leads to greatly reduced lateral resolution of the droplets (down to ~ 40 nm) with about an order reduction in the periodicity of the dewetted features.[149–151] The electrostatic force also alters the scaling between $\boldsymbol{\lambda}$ and **h** to $\boldsymbol{\lambda}$ ~

$\mathbf{h}^{1.5}$, in contrast to $\boldsymbol{\lambda} \sim \mathbf{h}^{2}$ (figure 3A), observed in the van der Waal's force driven instability of a film in air. Owing to a greater propensity of wetting of the substrate by the liquid mix, the dewetted polymer structures have very high contact angles (~ 140°), allowing possible fabrication of high curvature micro/nano lenses (figure 3B),[149–151] which is not possible in classical dewetting where the droplet aspect ratio is invariably low as it is governed by the equilibrium contact angle between the polymer and the substrate.

2.3 Effect of Visco Elasticity and Slippage on Dewetting

Films of long chain polymers beyond the entangle limit exhibit significant visco elasticity (VE) as well as finite slippage on smooth passive surfaces.[19,169] Interfacial slippage in a polymer melt is generally attributed to adsorption of molecules on the solid surface and is characterized by a slip length $\mathbf{b}=\boldsymbol{\eta}/\boldsymbol{\zeta}$, where $\boldsymbol{\eta}$=liquid viscosity and $\boldsymbol{\zeta}$ = coefficient of friction.[19] With increase in shear strain, the extant of disentanglement of the surface adsorbed molecules increases, which rapidly reduces the interfacial friction and enhances the slippage.[185] Significant slippage is observed when a film dewets on a substrate covered with end-grafted polymer chains of the same polymer (autophobic dewetting),[209–212] or a different one.[213,214] Autophobic dewetting is driven by a finite interfacial tension between the film and the grafted layer due to entropic effects,[209] and exhibits slip length as high as ~ 10 μm.[210–212] Interfacial slippage is also observed in films dewetting on a self-assembled monolayer (SAM) covered substrates due to the physicochemical roughness resulting from incomplete grafting, rather than entanglement or non-wettability, as the extant of slippage reduces with enhanced graft coverage.[213,214]

Reptation time ($\boldsymbol{\tau}_{\mathbf{rep}}$) is a key parameter related to visco elasticity (VE) of a polymer as it behaves like a deformable semi solid for $\mathbf{t} < \boldsymbol{\tau}_{\mathbf{rep}}$ and like a liquid only when $\mathbf{t} > \boldsymbol{\tau}_{\mathbf{rep}}$.[19,169] The effect of VE is pronounced when dewetting temperature is close to $\mathbf{T}_{\mathbf{G}}$ of the polymer.[168,175,177–

[179,184,186,189,191–206] Distinctive signatures of VE on a dewetting film, which are not observed in a purely viscous film with zero interfacial slippage are: i) formation of holes without rims in the initial stages of rupture;[173] ii) variation in dewetting velocity during different stages of hole growth (figure 4A);[168,173,177–179,193,199–202] iii) formation of highly asymmetric rims (figure 4B);[139,168,171,173,175,177–187,191–206] and iv) complete inhibition of hole growth beyond a critical hole radius ($\mathbf{R_C}$).[173] In a purely viscous film, a rim with uniform curvature appears right after rupture;[77,166,174,189,210] a constant dewetting velocity is observed; and holes grow fully and coalasce.[77,78,82,90] In a VE thin film, an exponential growth rate of hole radius, $\mathbf{R}(t) = \mathbf{R_0} \exp(\mathbf{t}/\boldsymbol{\tau_D})$ is observed in the early stages of dewetting (figure 4A), where $\boldsymbol{\tau_D} = 0.7\ (\mathbf{h_0}/V^*)$, and $\mathbf{V}^* = \boldsymbol{\gamma}/\boldsymbol{\eta}$ is capillary velocity,[173] which is in contrast to a power law growth rate observed in a purely viscous film.[76,134] During hole growth, the gain in the interfacial energy due to amplification of surface capillary waves is balanced by viscous dissipation which occurs both within the film and at the film–substrate interface.[173] In the early stages ($\mathbf{t}<\boldsymbol{\tau_{Rep}}$), the film is solid like and the amplification of the surface undulations lead to an elastic deformation of the film surface, resulting in Laplace pressure ($\mathbf{S}/\mathbf{h}$) at the edge of the hole. This causes the elastic stress to propagate across the film at the shear wave velocity as a long range plug flow without any localized accumulation of polymer, which manifests as holes without rims.[173] A hole continues to grow without a rim as long as interfacial dissipation remains insignificant till $\mathbf{R}$ attains a critical value $\boldsymbol{\Delta} = (\mathbf{h_0 b})^{\mathbf{0.5}}$.[168,195] For $\mathbf{R} > \boldsymbol{\Delta}$ dissipation starts dominating due to enhanced interfacial friction and the elastic shear stress gets screened at a finite distance from the center of the hole, paving the way for the appearance of a rim along the hole periphery.[168,173.195] In this regime ($\boldsymbol{\Delta} < \mathbf{R} < \mathbf{b}$), the increase in the capillary driving force, which is proportional to the perimeter of the hole, gets balanced by an increase in interfacial dissipation, resulting in a constant dewetting

velocity (figure 4A).[173,186] For **R** > **b**, increase in the rim width enhances the dissipation as a result of enhanced interfacial friction, which in turn leads to gradual reduction in dewetting velocity. For larger holes (**R**>10 μm) dewetting may stop completely due to higher rate of dissipation in comparison to rather low capillary driving force for hole growth.[191] Thus, VE of a polymer, which can be tailored by varying the degree of cross linking,[202] or by adding nano particles,[220] may lead to partial stabilization of an unstable thin film, as theoretically predicted by Safran and Klein.[219] The asymmetric rim shape in a VE film is attributed to several factors such as elasticity,[219,] strain hardening,[185,188] shear thinning of the polymer melt,[176] etc.

2.4 Directed Dewetting under Lateral Confinement

Preceding discussion shows that dewetting of a thin polymer film results in random structures, irrespective of the precise rupture mechanism.[30–47,74–214] In this section, we discuss how these random structures can be aligned by templating, which include the use of a topographically or a chemically patterned substrate.[44,46,47,221–263] Such an approach combines the essential features of top down soft lithography with bottom up self-organization.[44] Higgins and Jones first demonstrated the possibility anisotropic dewetting by simply rubbing the substrate in a specific direction with an emery paper before coating the film. The scratch marks guided the dewetting pathway of a PMMA film resulting in anisotropic, oriented structures.[221] Variety of ordered structures like nano-grooves, lines, droplets etc. have been obtained by brushing a smooth film before dewetting.[222] Spontaneous dewetting of a PDMS film deposited by wiping it with a paper pre-soaked dilute polymer solution in a specific direction resulted in aligned nano-channels with periodicity as low as 166 nm![223] Such approaches however fails to fabricated ordered instability structures with precise control of geometry, periodicity and fidelity, in a reproducible manner.

This can be achieved by dewetting a film on a chemically,[224–246] or topographically patterned substrate, typically fabricated by top down lithographic techniques.[247–259]

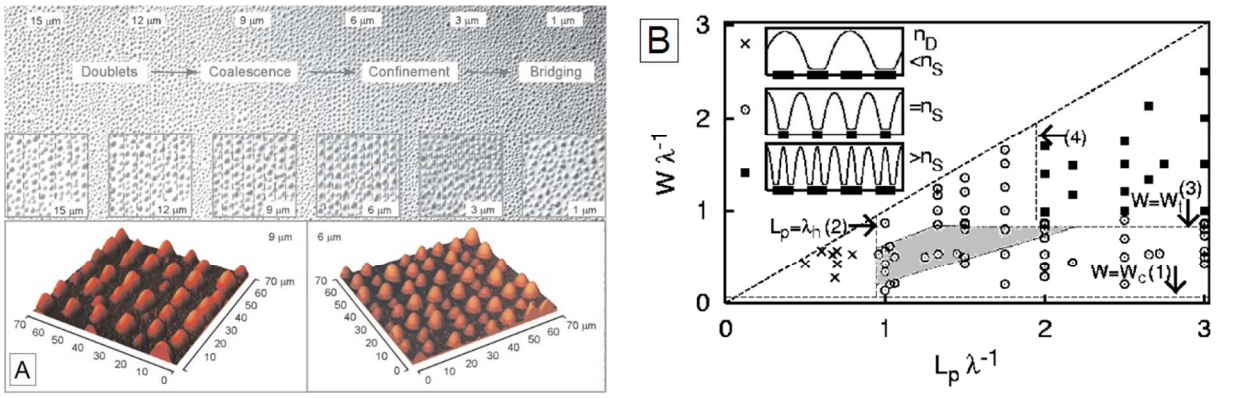

Figure 4: (A) Influence of substrate pattern periodicity on the final morphology (aligned, partially aligned and random droplet arrays) of structures resulting from dewetting of a 12 nm thick PS film. Optical micrographs and insets show transition from the doublet state (15-12 μm stripe width), to coalescence (9 μm), confinement (6 and 3 μm), and a heterogeneous morphology (1 μm) with bridging over multiple bands. Dashed lines (insets) indicate registry with the underlying chemical pattern period. AFM images (9 and 6 μm) highlight control of droplet size and spatial position. Reproduced with permission from ref. 233. Copyright 2002, American Chemical Society. (B) Morphology diagram for dewetting of a film on a striped surface. Broken lines, 1, 2, 3, and 4, denote the boundaries between different regimes at the onset of dewetting as shown in the figure by three symbols. The shaded region corresponds to good templating. Reproduced with permission from ref. 238. Copyright 2001, American Physical Society

2.4.1 Dewetting on Chemically Patterned Substrates

A chemically patterned substrate with alternate zones of less and more wettable areas acts as a closely packed array of chemical heterogeneity. For a thin film on such a surface, the term $(\partial\phi/\partial x)|_h$ in equation 2 becomes significant, as it triggers outward flow of polymer from less wettable to more wettable areas of the subrstrate.[238-242] The mechanism of flow is similar to Marangoni flow, except that the flow originates due to an in-plane gradient of free energy at the film – substrate interface, rather than at the free surface of the film.[238] The film generally ruptures over the lower wettability zones though there are examples where the film is seen to rupture over the more wettable domains, probably due higher local roughness of these patches.[224] The extant of ordering of the dewetted structures on a chemically patterned substrate depends on the commensuration between factors such as pattern periodicity (λ_P) and line width (l_P), film thickness (h) in addition to pattern geometry. Sehgal et al. experimentally explored the

possibility of obtaining fully and partially ordered structures by dewetting a spinodally unstable PS film (**h**=12 nm) on a chemically patterned substrate comprising progressively narrower stripes with $\mathbf{l_P}$ varying between 1–15 μm.[233] A strong anisotropy is superimposed on to the spinodal like dewetted features in the early stages of rupture by the underlying chemical patterns. The influence of $\boldsymbol{\lambda_S}$ and $\mathbf{l_P}$ on the final morphology is seen in figure 4A, as the final dewetted patterns vary from laterally coexisting double droplet array on the wider stripes ($\mathbf{l_P}$=12–15 μm); a single droplet array on the intermediate $\mathbf{l_P}$ stripes (9 μm); array of droplets with distorted oval shape for $\mathbf{l_P}$ = 6 μm; and complete loss of order for $\mathbf{l_P}$ < 3 μm.[230] A late stage bridging transition is seen on the narrower stripes, leading to coalescence of highly anisotropic drops across the less wettable patches to form well rounded structures due to reduced energy penalty.[233] In a recent paper the influence of lateral confinement on a dewetting thin film was investigated on a chemically patterned substrate with variable width of the less wettable area (1.5 to 15 μm), keeping the width of the more wettable area same (3 μm). When the less wettable patches were highly confined between the wider more wettable patterns, the film was seen never to dewet the substrate, as a large contribution from the in-plane curvature induced surface tension favours a low aspect ratio deformation at the free surface rather than droplets.[236] Julthongpiput et al. showed that the wettability contrast between the more and the less wettable domains ($\Delta\boldsymbol{\gamma}$) significantly influence the ordering process and perfect ordering is possible for $\Delta\boldsymbol{\gamma} \geq 43$ mJ/m^2. The quality of ordering gradually worsens with reduction in $\Delta\boldsymbol{\gamma}$ and is completely lost for values of $\Delta\boldsymbol{\gamma} < 4$ mJ/m^2.[237]

As several parameters influence the dewetting pathway and morphology on a chemically patterned substrate, simulations play an important role in understanding the system. Based on nonlinear simulations, the morphology and the dewetting pathways of films on chemically,

topographically and physico–chemically patterned substrates have been predicted by various groups,[238–246] many of which have subsequently been validated in actual experiments.[234-236] Simulations help in compiling pseudo morphology phase diagrams, which identifies zones with distinct boundaries that correspond to different types of structures (perfect order, disorder etc.) in the complex multi parameter space, significantly reducing experimental efforts.[239-243] Simulations show that the morphology of a dewetted film on a patterned substrate depends strongly on a competition among the various time scales (spinodal and heterogeneous) and length scales (spinodal, stripe width, periodicity, thickness) of the system.[238,239]A typical morphology phase diagram is shown in figure 4B (details available in the figure caption).

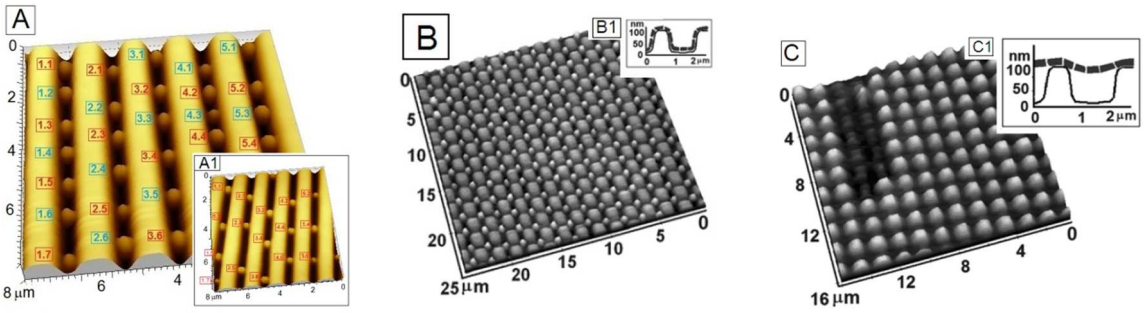

Figure 5: (A) Array of ordered alternating droplets of PS and PMMA obtained by spin dewetting. Inset shows only the PS droplets, after UVO induced degradation of the PMMA droplets. Reproduced with permission from ref. 251. Copyright 2014, American Chemical Society. (B, C) Influence of the nature of initial adhesion of a floated film on a topographically patterned substrate on the final pattern morphology. (B) On a patterned substrate comprising array of square pillars (periodicity: 1.5 µm in both X and Y directions, pillar height ~ 120 nm), the dewetted droplets position at interstitial locations surrounding the pillars, when nature of initial adhesion was conformal (inset B1). (C) The dewetted droplets position on top of the pillars for focal adhesion (inset C1). Film thickness in both cases is ~ 24 nm. Reproduced with permission from ref. 90. Copyright 2008, Royal Society of Chemistry.

2.4.2 Dewetting on Topographically Patterned Substrates

Dewetted features can also be aligned by using a topographically patterned substrate. However, things become more complicated on such a substrate as direct spin coating on a topographically patterned substrate results in a film with an undulating top surface and non-uniform thickness.[247,248] Such a film preferentially ruptures over the areas where it is thinnest.[251,253] On a topographically patterned substrate even the molecular weight and radius of gyration ($\mathbf{R}_g$) of the

polymer also influences the stability of the film. Rhese et al. showed that a film becomes unstable only when the thickness of the thinnest part of the film is below a critical thickness t_{Peak}, which varies as $t_{Peak} \approx 0.55\mathbf{R}_g$ for a PS film.[252] On the other hand, if the concentration of the polymer in the dispensed drop is extremely low, then the film ruptures and dewets during spin coating process itself, which is lately being referred to as *spin dewetting* and can result in well aligned structures on a topographically patterned substrate.[250,251] Recently an alternating droplet array of PS and PMMA has been realized based on sequential spin dewetting of the two polymer solution on a grating patterned substrate, which can be seen in figure 5A.[251]

Instead of directly spin coating the film on a topographically patterned substrate, in some cases a flat film of uniform **h** has been transferred on to a patterned substrate by floating.[90,255] In such cases, the dewetting pathway is strongly influenced by the nature of initial adhesion of the transferred film with respect to the substrate as two distinct initial configurations are possible: 1) *conformal adhesion*: when the film adheres closely to the contours of the substrate pattern (inset B1, figure 5B) and 2) *focal adhesion*: in case the film is in contact only with the protrusions of the substrate (inset C1, figure 5C).[90,255] A film in focal adhesion upon dewetting on a patterned substrate comprising an array of square pillars results in an array of droplets that occupy the interstitial places surrounding each pillar (figure 5B). In contrast, the droplets get positioned on top of the pillars in dewetting of a focally adhering film (figure 5C).[90] On a 2-D patterned substrate, perfect ordering occurs only over a narrow film thickness range.[90] Dewetting of polymer films on patterned surfaces with various other geometries have also been investigated.[251–263] Roy et al. showed that the extent of ordering as well as the evolution path way depends strongly on the height of the substrate features. In case the as cast film is continuous and thick, then even on a patterned substrate the film ruptures due to nucleation of random holes

uncorrelated to the substrate patterns.[259] A very recent paper reveals the possibility of obtaining aligned and ordered features from dewetting of a pre-patterned film on a template free, flat substrate when the remnant thickness at the valleys of the film after patterning is adequately low, so that the film preferentially ruptures over these locations ahead of surface tension induced flattening known as slumping.[261] Ordered dewetted patterns on topographically patterned substrates have been utilized for fabricating polymer thin film transistors, optical memory, and functional devices.[47,262,263]

2.5 Dewetting of a Thin Polymer Bilayer

Dewetting of a polymer bilayer is more complicated as it involves coupled evolution of two deformable interfaces.[264–295] Instability of a bilayer may either involve dewetting of a thin polymer film on a thick, viscous stable bottom layer,[264-273] or both the layers can become unstable sequentially.[274–288] The final dewetted droplet geometry over a non wetting soft bottom layer is given by the well-known *Neumann configuration*, instead of *Young's configuration*, which specifies the drop shape over a solid substrate.[264,265] In case the viscosity vis-à-vis the molecular weight of the bottom layer is high, then the system behaves identically to dewetting of a thin film on a rigid substrate. Brochard and coworkers, based on detailed theoretical analysis on dewetting and stability of a liquid bilayer have identified the existence of two collective modes of deformation in a stratified system, which are: 1) a transverse bending mode that is associated with vertical displacement, governed by the total surface tension; and 2) a longitudinal peristaltic mode which is associated with thickness fluctuations and horizontal displacement.[264,265,286–288] It is also argued in a low viscosity bottom layer, a visco inertial mode becomes dominant.[264] In case the bottom layer has viscosity comparable or lower than that of the dewetting top layer, then the rims formed around the holes penetrate into the bottom layer as a result of the vertical component of interfacial energy exerted on the soft substrate along the

contact line, resulting in a rim profile that is highly asymmetric with a steep decay inside the hole.[267] Faldi et al. reported that during dewetting of a Polycarbonate film on a 200 nm thick styrene-co-acrylonitrile (SAN) layer, polymer from under layer gets pulled into the rim and lowered the film thickness of the intact bottom layer within the hole.[266] Sferrazza et al. studies the early stages of evolution of a PMMA – PS bilayer coated on a silicon substrate using specular and off-specular neutron reflection and clearly observed the amplification of the thermally excited capillary waves at the polymer/polymer interface.[270] During dewetting of a PBrS film on a PS layer, Slep et al. showed that the PBrS core in the dewetted droplets is fully encapsulated by PS only when the bottom PS substrate thicknesses ($\mathbf{h_{PS}}$) is greater than $\mathbf{R_g}$. Only partial encapsulation is observed when $\mathbf{h_{PS}} < \mathbf{R_g}$. The Neumann contact angle after dewetting is also seen to increase with $\mathbf{h_{PS}}$.[272] Wang et al. investigated the dewetting of PS on both low and high viscosity PMMA films ($\boldsymbol{\eta_{PMMA}}$). On high $\boldsymbol{\eta_{PMMA}}$ bottom layer, the dewetting speed is found to be constant and independent of the PS layer thickness. In contrast on a liquid like PMMA layer (low $\boldsymbol{\eta_{PMMA}}$), the radius of the dewetted holes grows as $\mathbf{t^{2/3}}$, (t is annealing time), and depends on the thickness of both the layers.[273] With a PVP/PS bilayer coated on a silicon wafer, Kang et al. observed a layer inversion during dewetting as a higher surface energy PVP preferentially wets the silicon substrate and thus fills up the holes created in the PS film and spreads along the substrate, dislodging thee bottom layer completely.[274] Similar layer inversion is also observed in Poly(4-vinylpyridine)/Polystyrene bilayer thin films.[285]

Chattopadhyay et al. in an interesting combinatorial study involving a conducting – insulating polymer bilayer of PS and P3OT found a stability transition around a critical P3OT film thickness of 175 nm. Initially, with gradual increase $\mathbf{h_{P3OT}}$, progressively thinner PS top layer is seen to become stable, as the bottom P3OT layer screens the unfavorable van der Waals (VDW)

interactions between the PS film and the Silicon substrate. However, as $\mathbf{h_{P3OT}}$ exceeds 175 nm, reappearance of instability in the PS layer is observed. This transition is attributed to thickness dependent bipolaronic changes in properties such as polarity, polarizability and conduction bands of the semiconducting P3OT.[275] Paul et al. studied dewetting of a poly(*tert*-butyl acrylate) (PtBA) and trisilanolphenyl-POSS (TPP) bilayers and observed fractal nanofiller (TPP)-rich aggregates at the bottom of the scattered holes upon prolonged annealing, as the holes reach down into the PtBA layer.[277,278] de Silva et al. showed that there is a switching of the instability mode in a PMMA on PS bilayer coated on Silicon by simply changing the film thickness. While thin PMMA film on a thick PS film becomes unstable due to dispersion forces, thin PS layers buried under PMMA film dewets spinodally due to long-range forces.[280] Recently, Xu et al. experimentally studied different aspects of bilayer instability in great details.[282–284] In a PS-PMMA bilayer on a non wettable silicon substrate, the time of formation of the holes and the dewetting velocity are key in determining whether the film ruptures at the liquid – liquid or liquid – solid interfaces.[282] They also reported the formation of highly anisotropic and faceted holes in dewetting of the upper PS layer when viscous dissipation is dominated by the upper PS film. This happens when the layer has higher viscosity and lower thickness, which in turn gives rise to strong interfacial slippage, resulting in broad rims around initially circular holes. Subsequent growth occurs selectively in the directions of lower viscous resistance leading to the anisotropy.[283] A bilayers with ultrathin PMMA layer under a thin PS layer always exhibit a strong deformation at the polymer/air interface over a non-deforming polymer/polymer interface. In contrast, the polymer/polymer interface deforms easily when the bottom PMMA layer is thicker and has lower viscosity.[282] Based on dewetting of a PS film submerged below a continuous layer of conducting polymer, P3HT, they obtained a undulating P3HT conducting

skin covering the isolated PS droplets.[284] Neto et al. utilized dewetted PMMA droplets on an intact PS layer for preferential and controlled adsorption of protein molecules on a surface.[279]

As bilayers are extremely sensitive to initial conditions, accurate simulations play a crucial role in predicting the morphology, the evolution path way and more importantly, the morphology of the interface during and after dewetting, which cannot be directly visualized using real space imaging techniques.[286–288] Bandyopadhyay et al. theoretically showed that a likely transition from the squeezing and bending modes at late times can occur when the film thicknesses either corresponds to the minima of the dominant growth rate or which switching between the high- and low-wavenumber regimes occur.[287] They also presented the short and the long-time dynamics, interfacial morphologies, and the rupture and dewetting pathways based on nonlinear simulations, which suggests that over longer durations the intermolecular and viscous forces can profoundly modify the initial mode of instability and its growth rate, resulting in complex late stage morphologies such as embedded droplets, inversion of top and bottom phases, and encapsulation of one layer by the other film.[288]

When a polymer bilayer is dewetted on a topographically patterned substrate, it is possible to have a variety of exciting structures such as array of core-shell droplets, array of droplets under intact top layer, aligned undulating threads, co-existing ordered droplets arrays of both polymer etc. can be obtained depending on the thickness ratio and the initial morphology of the bilayer.[289] Based on nonlinear simulations, the likely morphology of a polymer bilayer on chemically and topographically patterned substrates have been predicted by Bandyopadhyay and Sharma.[290,291] Their work provides a comprehensive understanding of the system and highlights the possibility of obtaining variety of interesting and complex, dissipative patterns based on an interplay of

various parameters such as pattern geometry, dimension, thickness and interfacial tension of both the layers, substrate wettability etc. [290,291]

Ding and coworkers have explored the evolution of a polymer bilayer with a topographically structured interface.[292-295] On a thick patterned PMMA layer, they observed two sequential events of capillary instability, which lead to PS stripes segregated on the PMMA mesas and PS threads confined in the PMMA trenches. [292] The kinetics of the capillary breakup is a strong function of the duty ratio and the viscosity ratio of the two polymers and is dominated by the property of the more viscous component.[293] When both the layers are thin, the PS (or PMMA) stripes confined within PMMA (or PS) trenches breaks up, either nucleated, out-of-phase, or without clear phase correlation depending on the geometry, residual layer thickness and molecular weight ratio between the two polymers.[294] They observed a vertical pattern decay in dewetting of a nano imprinted bilayer, and formation of final structures in a direction orthogonal to that of the initial stripes, leading to partially ordered structures.[295]

2.6 Perspective on Thin Film Dewetting

In this section we have presented a short overview on how research on spontaneous rupture, instability and pattern formation in thin viscous films has evolved over the last two decades. Though dewetting of simple liquids such as water or organics solvents were known for a long time, use of a Polymer by Gunter Reiter in 1992 as a model system for experimentally studying dewetting of a thin film revolutionised the field, with renewed interest. There are several advantages of using a polymer over a simple, regular liquid, as the evolution can be frozen at an intermediate stage by mere switching of temperature. The structures, at least during the time scales of experiments were absolutely stable, as evaporation, an inherent problem in any liquid is completely eliminated in a polymer. The solid like frozen structures also paved the way for

characterizing the dewetted features by techniques such as AFM and SEM, as well as the scattering based reciprocal space techniques, each one of which have given far more insight into the physics of the system than simple optical microscopy based observations.

Alongside novel and elegant experiments, theoretical developments in the field also matured with simulated predictions that could be directly compared with experimental observations. Despite the in-depth understanding in the field, certain ambiguities still remain, which we have highlighted in our discussion. For example, many groups have reported (and therefore, repeatability is unquestionable!) dependence of $\boldsymbol{\lambda_m}$ or $\mathbf{N_m}$ with $\mathbf{h}$ that is identical to theoretical predictions in pure spinodal dewetting, in much thicker films where nucleation seems to be the sole reason for rupture! Similarly, though theoretical predictions match experimental findings rather well, even in terms of morphology, most of the models consider Newtonian behaviour of the polymer melt, which for long chain molecules is hard to accept! Another major issue that many researchers have not accounted properly is the confinement induced reduction of the $\mathbf{T_G}$ during actual dewetting, which is likely to have strong influence on the rupture time scale and dewetting velocity.

The ordering of the dewetted structures on topographically patterned substrate is indeed a novel meso patterning strategy, and offers much higher degree of morphology control and flexibility as compared to classical top down methods. Still it is unlikely that this approach will find more favour with users for nano patterning over existing Soft Lithography methods, due to the sensitive nature of the final morphology on initial conditions and delicate experimental protocols. However, such method can be indeed useful for functional materials for novel applications such as imaging, sensing, water harvesting, sustained drug release etc., particularly exploiting the instability of bilayers which has the potential to fabricate embedded or submerged

structures with definite interfacial architecture that is impossible to achieve by any existing top down method.

3.0 Contact Proximity induced Instability in Thin Elastic Films

3.1 Elastic Contact (EC) Instability: Theory

In this section, we review contact proximity induced instability observed in a soft solid film that exhibits room temperature elasticity (category 2).[296–345] In contrast to category 1 instability involving dewetting, where the excess interfacial free energy within the film causes the instability, in the present case instability results due to an attractive interaction between the free surface of the film and another rigid surface (the contactor), when the two are in close proximity. Unlike category 1, where surface tension opposes the growth of instability, in a soft elastic film the role of surface tension is rather insignificant and the instability is opposed solely by the elasticity of the film. Further, in this case instability is associated with solid state deformation and does not involve any advective transport of material by flow or diffusion. Deformation of a thin elastic film confined between two surfaces is important in various settings such as adhesion, friction,[296] peeling of a pressure sensitive adhesive,[297] crazing behavior of glassy polymers,[298] interfacial bonding in composite materials etc.[299] EC instability is distinct from instabilities in pre-stressed solid films engendered by the elasticity of the film itself,[300] or due to large nonlinear plastic deformation.[301] Despite strong morphological similarities, EC instability is completely different from the classical *Saffman-Taylor* instability observed in a *Hele Shaw* cell, where flow-driven fingering patterns form at a moving interface between two viscoelastic liquids.[302] In EC instability, the destabilizing energy remains stored within the flexible matrix of the elastic film itself and once the contactor is withdrawn, the stored energy is released and the film surface restores back to its original flat morphology.[303,331]

The elastic strain energy per unit area of a deformed film surface (***U***) is given by:[303–310]

$$\boldsymbol{U} \approx \mu\, h\, (\partial v/\partial x + \partial u/\partial z)^2 \qquad (7)$$

where, $\boldsymbol{\mu}$ is the elastic modulus, u and v are the components of the displacement field in the lateral (***x***) and the normal (***z***) directions, respectively.[303,304] By considering the characteristic orders of the length scales as $\boldsymbol{x}\sim\boldsymbol{\lambda}$ (instability length scale), $\boldsymbol{z}\sim\boldsymbol{h}$ (film thickness) and $\boldsymbol{v}\sim\boldsymbol{\delta}$ (vertical amplitude of the pattern) in equation (7), in conjugation with the continuity equation [$\partial u/\partial x + \partial v/\partial z = 0$], provides a scaling relation for the stored elastic energy due to the shear and normal deformations of the film surface as: [303–310]

$$U \approx \mu\, h\, \delta^2(\lambda^{-1} + \lambda H^{-2})^2 \qquad (8)$$

It can be seen in equation (8) that the energy penalty for deformation of the film surface increases for both very short ($\boldsymbol{\lambda} << \mathbf{h}$) and for very long ($\boldsymbol{\lambda} >> \mathbf{h}$) wave undulations, and therefore the minimum energy configuration ($\partial U/\partial\lambda = 0$) is attained only when $\boldsymbol{\lambda} \approx \boldsymbol{h}$. A numerical pre-factor close to 3 for the scaling relation ($\boldsymbol{\lambda} \approx 2.96\mathbf{h}$) is obtained based on detailed LSA.[303-306] The analysis also shows that $\boldsymbol{\lambda}$ is independent of the elastic modulus of the film at the onset of instability as well as the surface tension of the contactor,[303,304] which has been experimentally verified.[311,330–334] The pre-factor may increase significantly to values higher than 3 in films thinner than ≈ 1 μm due to enhanced effect of surface tension.[311] Nonlinear simulations based on complex energy minimization have been used predict and understand the mechanism and pathways during approach and de-bonding of a rigid contactor to/ from a soft interface. Simulations also show the existence of an adhesion-debonding hysteresis, due to the energy barrier associated with the pinning of the metastable patterns with the contactor surface during debonding.[306,307] Finite element based models have also been used to capture the nonlinear regimes of elastic instability.[312,313]

3.2 Elastic Contact Instability: Experiments

Experimentally, EC instability in thin films has been studied in three distinct geometries: 1) peeling a rigidly bonded convex or cylindrical contactor from the film, which is similar to the well known probe tack test geometry;[314–321] 2) peeling a flexible contactor from one side of a flat film;[322–329] and 3) bonding – debonding of a flat rigid contactor parallel to the film surface.[311,330–332] In experiments with a rigidly bonded convex contactor, the film becomes unstable at a critical nominal strain as the contactor is detached under a constant tensile load and undulations appear along the circular contact line at the onset of instability.[314–316] The perturbations become prominent with inward growth of the elastic fingers due to reduced lateral confinement at large strains. At higher tensile loads, a cohesive fracture results half way between the two contacting surfaces. The morphology of the patterns are strongly influenced by the extent of imposed confinement and the mode of cohesive failure can vary from simple interfacial fracture to cavitation in a fibrillated structure.[315,316]

In peeling experiments with a flexible contactor, which typically is a microscope cover slip, the interfacial crack propagates in the direction of peeling, resulting in undulating elastic fingers at the crack front, which can be seen in figure 6A. The fingers form due to non-uniform deformation at the contact line caused by adhesive stresses, as spatially varying deformations correspond to a lower energy configuration for the system.[322,323,327,328] The wavelength ($\boldsymbol{\lambda}$) of the patterns varies linearly with $\mathbf{h}$, and is found to be independent of the shear modulus ($\boldsymbol{\mu}$) of the film, the flexural rigidity ($\mathbf{D}$) of the contactor, as well as the surface energy of the film and substrate.[322,327,328] However, the amplitude of the fingers ($\mathbf{l_a}$) reduce with increased rigidity of the contactor. The fingers become highly irregular when $\mathbf{l_a}$ exceeds $\boldsymbol{\lambda}$, and tend to split, resulting in isotropic ripple-like structures (figure 6A4).

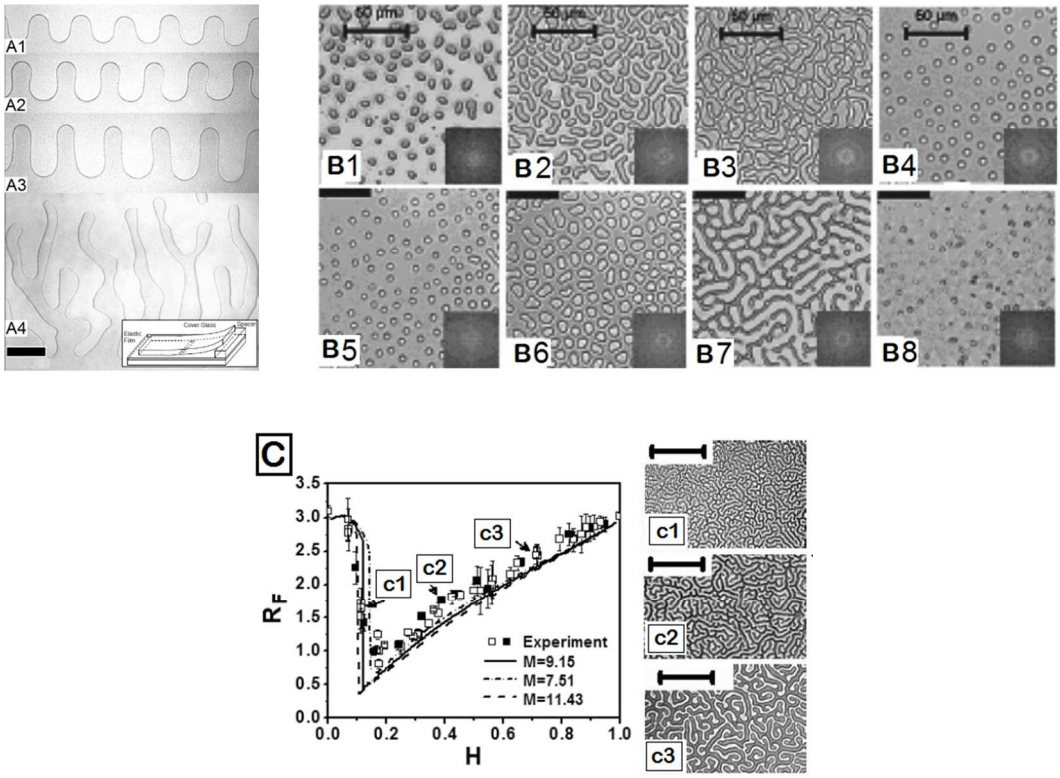

Figure 6: (A) Contact instability in a thin elastic film with flexible glass contactors having different flexural rigidities. Film thickness in all cases (A1 – A4) 150 μm and shear modulus 1.0 MPa. (A1), (A2), and (A3) correspond to cover glasses having flexural rigidities 0.02, 0.09, and 0.2 Nm, respectively. (A4) A highly irregular growth of fingers is observed for a glass contactor having high flexural rigidity of 1.0 Nm. Scale bar 500 μm. Reproduced with permission from ref. 322. Copyright 2000, American Physical Society. (B) Morphological evolution during bonding (B1–B4) and debonding (B5–B8) of a rigid stamp to a 3.2 μm thick elastic film. The evolution sequence comprises of: (B1) isolated columns with fractional contact area $\alpha \sim 0.25$, (B2) elongated columns and coalescence, $\alpha \sim 0.51$, (B3) labyrinths, $\alpha \sim 0.68$, and (B4) isolated cavities, $\alpha \sim 0.76$; (B5) isolated cavities, $\alpha \sim 0.74$, (B6) expanded cavities approaching coalescence, $\alpha \sim 0.56$, (B7) labyrinths, $\alpha \sim 0.37$, and (B8) isolated columns approaching complete detachment, $\alpha \sim 0.03$. Scale bar 50 μm. Reproduced with permission from ref. 311. Copyright 2006, American Physical Society. (C) Variation of R_F as a function of H (film thickness ratio) in the contact instability of an elastic bilayer, when a softer film is stacked on top of a stiffer film. For this particular case, M = 5.86. The insets show the morphology of the bi-continuous structures corresponding to the points marked on the plot. Reproduced with permission from ref. 335. Copyright 2007, WILEY-VCH Verlag GmbH & Co.

Also, for a specific value of **D**, there exists a critical **h** beyond which no meniscus instability is observed.[322,323] In case the contactor is peeled from a film which has multiple incisions, the crack moves intermittently as the edges create crack-initiation barriers. The dynamics of crack propagation depends strongly on the depth, geometry and spacing of the incision patterns.[325,326] The resistance to crack propagation leads to significant enhancement of fracture energy between

the film and the contactor. This concept has led to the development of a new class of reusable pressure sensitive adhesives. The extent of adhesion can be enhanced by several orders in the presence of sub surface liquid filled micro channels. The additional crack arresting property of the channels can be attributed to capillarity induced surface stresses.[329]

In the parallel configuration, the contactor is first brought in contact of the film and subsequently de-bonded, which allows tracking of the morphological transformation during a complete bonding – de-bonding cycle as a function of the inter surface separation distance.[311,330,332] The onset of instability during bonding is with the formation of isolated columns, which transform into bi-continuous labyrinths and then isolated holes with progressive approach of the contactor (figure 6B, frames B1 – B4).[311,330] An exact opposite sequence with hysteresis in separation distance is observed during de-bonding (figure 6B, frames B5–B8). Interestingly, λ remains nearly invariant across all morphologies due to the pinning of the initial instability structures to the stamp in a local thermodynamic metastable state.[311] A soft flexible stamp however fails to cause any surface instability as it succumbs to the attractive inter surface interaction, forming instantaneous conformal contact with the film surface.[334]

3.3 Contact Instability of Elastic Bilayer and Two Interacting Films

Additional controls on the pre-factor ($\mathbf{R_F}$) in the scaling relation between λ and h, which remains nearly constant at $\mathbf{R_F} \approx 2.96$ in a single layer film, can be achieved by using an elastic bilayer comprising of two stacked elastic films with different shear moduli (μ_1, μ_2; shear modulus of bottom and top layers respectively) and thickness (h_1,h_2; thickness of bottom and top layers respectively) due to coupled deformation at the interface between the two layers.[335–337] The magnitude of $\mathbf{R_F}$ is strongly influenced by the stacking order of the films. When a softer film is placed on top of a stiffer film, $\mathbf{R_F}$ assumes values lower than 3 and can be as low as 0.75 under

specific conditions (figure 6C).[335] This allows significant downsizing in pattern dimensions.[335] A stiffer film on top of a softer film results in increase of $\mathbf{R_F}$ to values higher than 3, as the horizontal deformation at the interface results in an effective slip-like effect for the top film.[335,337]

When two soft elastic films with dissimilar shear modulus approach each other, a co-operative instability mode at a common λ evolves, which has a non–linear coupling between the vertical and parallel displacements in both the films.[338–341] Nonlinear simulations show that λ of the patterns increases with increased compressibility of the film and is dominated by the film with higher compressibility. In the event the two interacting films having equal shear moduli, **λ** depends on the relative thicknesses of the films.[340] In case the thicknesses of the films are substantially different, the overall **λ** is found to be intermediate between **λ** of each film had they been in contact with a rigid contactor.[340] For highly compressible films the instability is almost absent as simple jumps to uniform conformal contact results.[338]

3.4 Elastic Contact Lithography

Elastic Contact Lithography (ECL) an approach that aims to align the random instability patterns by imposing lateral confinement.[331–333, 342–345] Strategies adopted in this regard include: 1) use of a topographically patterned stamp;[331–333,342,345] 2) using a topographically patterned substrate; [343,344] and 3) shearing of a flat stamp while it is in contact with the film.[331,332] ECL has been implemented in an elastic bilayer to derive the advantages of feature dimension miniaturization as well.[345] The key advantage of ECL over existing soft lithography methods is the possible creation of patterns with distinct morphologies by controlling the commensuration between the **λ** of the film and the $\boldsymbol{\lambda_P}$ of the stamp/ substrate, along with their in-situ manipulation, reconfiguration and potential ability to create structures on demand.[331,332,345]

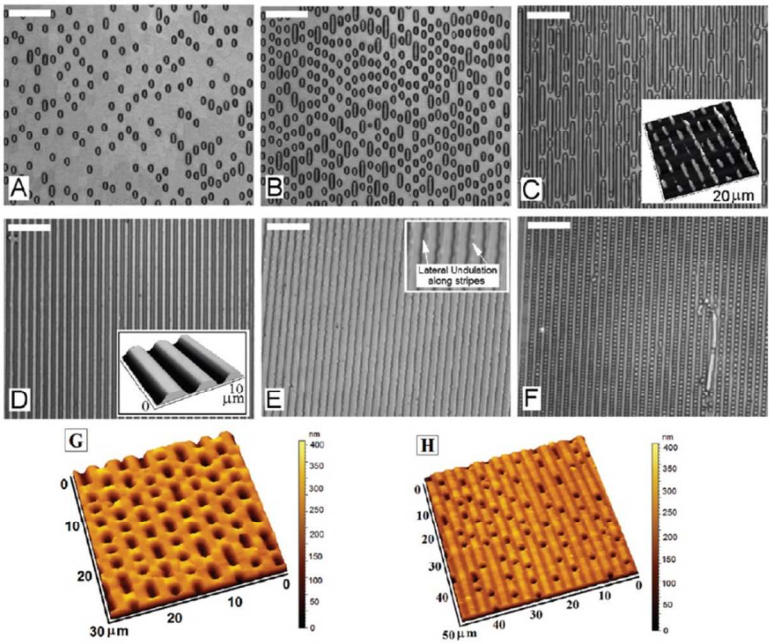

Figure 7: Morphological evolution sequence (frames A−H) of instability patterns in an elastic bilayer with h = 3.498 µm; M = 9.15; H = 0.16 in proximity of a grating stamp with λ_P = 3 µm, l_P = 1.5 µm, and h_P = 200 nm. (A) Onset of instability is with isolated columns with nearly circular diameter; (B) more number of columns appear below the stamp protrusions; (C) stretched columns under stamp protrusions start joining up; (D) positive replica of the stamp pattern, with inset showing an AFM image of the structures made permanent at this stage; (E) undulations along the periphery of the stripes as the stamp approaches beyond the level of a positive replica formation, with inset showing the details; (F) aligned array of circular holes isolated by stripes, resulting from bridging of the secondary instability structures in the form of undulations on the stripe edges; (G) AFM image corresponding to the stage shown in F; (H) gradually disappearing holes leading to the formation of a perfect negative replica in the final stage of approach. The scale bar in all optical microscope images A−F corresponds to 15 µm. Reproduced with permission from ref. 345. Copyright 2012, American Chemical Society.

Figure 7 shows the morphological evolution sequence when a grating stamp approaches a soft elastic bilayer. The onset of instability is with the formation of aligned columns (figure 7A), which transforms to a positive replica of the stamp (figure 7D), through various intermediate stages. Further approach of the contactor beyond the stage of a positive replica results in the appearance of periodic undulations along the periphery of each stripe (figure 7E, inset) which eventually bridge across adjacent stripes, forming bifurcated 2D structures (figure 7F,G) comprising array of pico- litre beakers. Formation of such ordered 2D structures takes place only when $\lambda \approx \lambda_P$ and has been observed in single layer elastic films, [331,] metal coated thin elastic films,[342] as well as thin films of hydrogel.[333] Similar ordered 2D patterns have also been obtained

using a grating substrate and a flat contactor, where the influence of the substrate "bleeds" through the film to the free surface, resulting in ordered, aligned patterns.[345,346] In case there is a mismatch between λ and λ_P, the film rather faithfully adheres to the instability length scale corresponding to 3 times the film thickness, paving the way for possible fabrication of structures with variable duty ratio.[331] The patterns are made permanent by an UV ozone exposure which results in a stiff crust layer that prevents the relaxation of the film even after withdrawing the contactor. Patterns can also be aligned by shearing a flat stamp while in contact with the film in a specific direction, thereby transforming the random labyrinths into aligned stripes.[331]

3.5 Perspective on Elastic Contact Instability

In this section we presented a class of instability that is specific to Soft Solid films that exhibit room temperature elasticity. The basic theoretical understanding on the genesis of instability is rather well understood. However the precise origin of the bonding – debonding hysteresis, additional stresses arising within the film matrix during debonding as a consequence of stretching, and whether modulus of the film in any way influences the extent of hysteresis is yet to be fully resolved. From the standpoint of patterning, ECL has great potential to become a true *beyond master* patterning technique, where the final pattern is no longer limited to a mere negative replica of the stamp. Its ability to for an array of 2-D holes (or beakers!) starting from a single stamp is truly outstanding. However, freezing the instability patterns by UVO exposure severly hinders its practical applicability in terms of patterning a large area. As of now, the material that has been used for most EC experimental studies is cross linked PDMS. In future if similar instability mediated structures can be made in a silicon free elastomer, then subsequent pyrolysis might enable fabrication of carbon nano structures following this approach. The array

of beakers can further be used as nano reactors for synthesis of colloidal particles or single crystals with high degree of mono dispersity.

4.0 External Field mediated Instability

In this section we review category 3 instability engendered by the application of an externally applied force field such as an electric field,[347–381] or a thermal gradient,[382–389] or in some rare cases, triggered by mere proximity induced effects itself![390–396] This type of instability is observed in both glassy as well as elastic films. A higher strength of the external filed and a long range of electrostatic interactions can destabilize much thicker (~ few hundred nm) films following this approach, as compared to category 1 instability setting.

4.1 Electro Hydrodynamic Instability (EHD)

The effect of an external electric filed on the surface of a viscous film was first shown in 1897 by Swan.[346] However, it was quite recently that EHD instabilities were utilized for patterning a polymer thin film,[347] where an electric field is applied across a polymer film sandwiched between two electrodes separated by a spacer, in a capacitor geometry.[347–382] The applied voltage between the two electrodes results in an excess electrostatic pressure ($\mathbf{p_{EL}}$) at the free surface of the film and amplifies the interfacial capillary fluctuations in the direction of the field.[347–350,357–360,369–376] Based on minimization of stored energy within the capacitor under a constant applied voltage **U**, an expression of $\mathbf{p_{EL}}$ can obtained as:[34]

$$\mathbf{p_{EL}} = -\,\varepsilon_0\,\varepsilon_P\,(\varepsilon_P - 1)\,E_P^2 \qquad (10)$$

where $\boldsymbol{\varepsilon_0}$ is the dielectric vacuum permittivity, $\boldsymbol{\varepsilon_P}$ is the dielectric constant of the polymer and $\mathbf{E_P}$ is the strength of the electric field in film. The corresponding dispersion relation in a system dominated by electrostatic forces is given as:[348]

$$\tau = -\,(h_0^3 / 3\eta)\,[\gamma q^4 + q^2\,\partial(p_{EL})/\partial h] \qquad (11)$$

where h_0 is the initial film thickness, η is the viscosity and q is wave vector. A dependence of $\tau \sim q^2$ is a clear signature of a dissipative system.[348] The necessary condition for the amplification of the fluctuations is $\tau > 0$, which becomes possible only when $\partial(p_{EL})/\partial h < 0$. The expression for the corresponding wavelength (λ) of the fastest growing mode is obtained as:[348]

$$\lambda = 2\pi \sqrt{\frac{\gamma[\epsilon_p d - (\epsilon_p - 1)h]^3}{\epsilon_o \epsilon_p (\epsilon_p - 1)^2 U^2}} = 2\pi \sqrt{\frac{\gamma U}{\epsilon_o \epsilon_p (\epsilon_p - 1)^2}} E_p^{-3/2} \qquad (12)$$

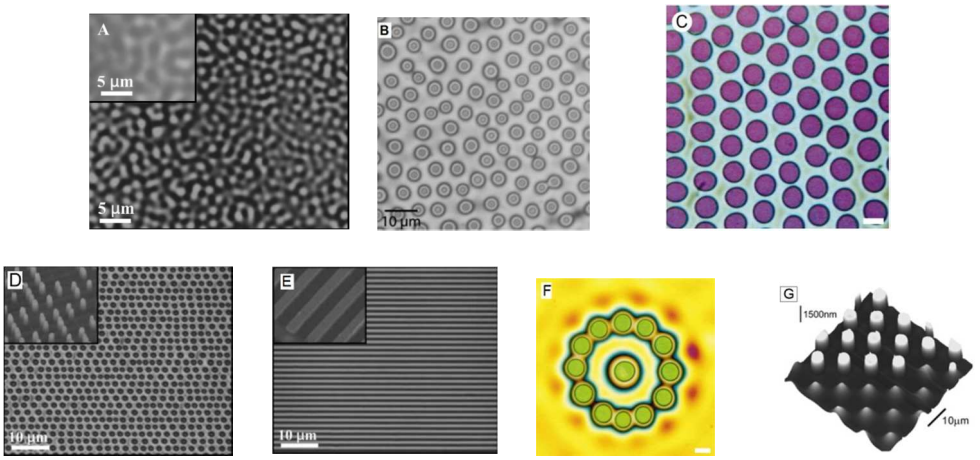

Figure 8: (A) Initial undulations in the form of a low amplitude capillary wave on the of a 100 nm thick Poly Venyl Acetate film. Reproduced with permission from ref. 354. Copyright 2010, WILEY-VCH Verlag GmbH & Co. (B) Pattern formed in an electric field instability with low filling ratio (f=0.25) in a 78 nm thick PS film, heated for 20 h at 170^{O}C. The applied field strength is 80 V. The columns are laterally disconnected and have a narrow diameter distribution. Reproduced with permission from ref. 352. Copyright 2006, WILEY-VCH Verlag GmbH & Co. (C) A denser packing of columns leading to perfect hexagonal order in a 193 nm thick PS film annealed for 18 h at 170 ^{O}C with an applied voltage U ~ 50 V (scale bar 5μm). Reproduced with permission from ref. 347. Copyright 2000, Nature Publishing Group. (D, F) Pattern Replication on a Ethyl Cellulose Film with patterned top electrode (Line Grating): (D) Aligned pillars for higher gap spacing and (E) Positive Replica of stamp for lower gap width. (D, E): Reproduced with permission from ref. 354. Copyright 2010, WILEY-VCH Verlag GmbH & Co. (F) A second-order effect observed in a nucleated instability under a point protrusion in the top electrode, in the form of a ring of 12 columns on a circle with a radius of 2λ. (scale bar 5μm). Reproduced with permission from ref. 347. Copyright 2000, Nature Publishing Group. (G) AFM scan showing the boundary between stable and unstable equilibrium surface modes, in a Spatially modulating electric filed. Reproduced with permission from ref. 356. Copyright 2009, Royal Society of Chemistry.

In experiments, early stages of EHD instability is manifested with the appearance of surface undulations (figure 8A).[347] The amplitude of the fluctuations grow with time in the direction of the applied field, eventually leading to the formation of columns that span the entire gap spacing (**d**) between the top electrode and the film (figure 8B).[347–361,363–376] The columnar configuration

corresponds to lowering of the total electrostatic energy of the capacitor compared to an initially flat film with an air gap. The extant of ordering of the columns depends largely on fill factor $\boldsymbol{f}$ ($\mathbf{h}/\mathbf{d}$), in addition to field strength and surface tension.[347,352,360] Columns with perfect hexagonal symmetry and denser packing results at higher values of $\boldsymbol{f}$ due to higher degree of electrostatic repulsion between equally charged undulation peaks (figure 8C).[347,360] For $\boldsymbol{f} > 0.5$, the film remains partially interconnected even after column formation and final morphology is strongly influenced by late stage ripening.[352,360] At very high $\boldsymbol{f}$ (> 0.75) coalescence of columns leads to phase inversion, resulting in cavities in a continuous polymer matrix.[352,361,371]

Additional ordering of the patterns can be achieved by using a topographically patterned top electrode[347,352–354] or a patterned substrate.[361] As a result of periodic spatial variation in $\mathbf{d}$ vis-à-vis the electrostatic field strength over the film surface, the emerging patterns evolve along the contours of the stamp/substrate. Depending on $\boldsymbol{f}$ and the relative magnitudes of $\boldsymbol{\lambda_P}$ and $\boldsymbol{\lambda}$, the final patterns either comprise an array of aligned pillars (figure 8D) or a positive replica of the stamp (figure 8E).[347,352–354,359–361] On the other hand, a nucleated instability under a single heterogeneous patch is seen to result in a rosette of columns along a circle with radius $\mathbf{r} \approx 2\boldsymbol{\lambda}$ (figure 8F). Such an unique morphology is attributed to the suppression of the nearest neighbor undulations due to flow of polymer towards the point of nucleation, which allows the second order effects to amplify, resulting in the formation of rosette of columns at $\mathbf{r} \approx 2\boldsymbol{\lambda}$.[347,360] EHD Lithography has been utilized for patterning low viscosity photo curable polymers like epoxy, vinyl ether, acrylate, and thiol-ene,[351,354] and sol gel based inorganic thin films.[353] Since EHD produces a positive replica, stamp release related problems encountered in typical soft lithography methods are automatically eliminated in this technique.[353]

A thin polymer film can also be destabilized by an in-plane,[362] or a spatially modulating electric field.[356] In plane electric field results in the formation of isolated polymer droplets with a narrow size distribution and spatial ordering, resembling dewetted patterns.[362] On the other hand a spatially modulating field exhibits two distinct regimes with a clear boundary that is defined by the dimensionless field strength (τ) and the dimensionless lateral field modulation (ε) in the phase space (figure 8G).[356] While the first regime exhibits stable surface undulations with finite amplitudes matching the periodicity of the imposed field, in the second regime the film breaks up into pillars localized around the region of maximum field strength. A finite conductivity can lead to patterns with smaller wavelength and faster growth rates in leaky dielectric liquids.[370]

Extremely interesting to point out that Chou and co-workers observed the formation of pillars in polymeric thin films in very close proximity to another rigid substrate, without the application of any electric field.[390–395] The mechanism is scientifically intriguing as the key driving force for the appearance of the structures is believed to be the internal localized electrical field generated between the contactor and the viscous film. The generation of the electric field is attributed to image charge-induced electro hydrodynamic-instability (ICE) model.[390,391,396] In this method, known as Lithographically Induced Self Assembly (LISA), Rayleigh–Benard instability due to thermal convection, Benard convection driven by surface tension, surface charges accumulated on the film and the image charges on the contactor are argued to determine the final pattern morphology.[392,395] The feature size can be minimized by filling the space between the contactor and the film by a liquid, as this reduces interfacial tension.[393] Further, time resolved experiments have shown that the columns appear in a sequential manner,[392,393] which is in clear contrast to elastic contact or EHD instability where the entire film evolves concurrently. The pillar forming cascade in LISA is attributed to an in plane variation of the pressure gradient which is maximum

at the corners below the stamp and is higher along the edges, where the columns appear first.[392] By using a topographically patterned stamp, extremely well aligned patterns with sub 100 nm lateral resolution has been created by LISA.[394]

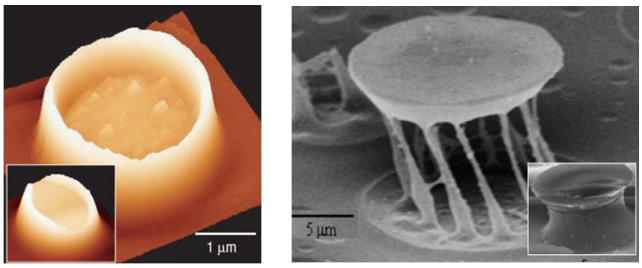

Figure 9: (A) AFM image of a single column after removing the PS core by washing in cyclohexane. Inset shows the column morphology before removal of the core. reproduced with permission from ref. 366. Copyright 2002 Nature Publishing Group, 2002. (B) A single "cage" formed due to combination of dewetting and EHD in a PMMA – PS bilayer, after the washing the composite PS – PMMA columns in cyclohexane to preferentially remove PS. Inset shows the composite columns before removal of the PS core. reproduced with permission from ref. 367. Copyright 2006, American Chemical Society.

4.2 Electric field Induced Patterning of Polymer Bilayers

EHD instability in a thin polymer bilayer has been investigated in two distinct configurations: without and with air gap between the film and the contactor. In case there is no air gap, the growth rate of the instability is much faster and the feature size reduces significantly due to reduced interfacial tension.[363,364] On the other hand, in presence of an air gap, either of the film–film or the film–air interfaces become unstable preferentially, resulting in the formation of hierarchical structures that exhibits a combination of two independent characteristic lengthscales.[365–368,372–376] Generally, the film – film interface is slow to evolve due to higher viscous dampening compared to the film–air interface.[365] Depending on the strength of the field, it's temporal modulation as well as the stacking order of the polymers, distinct morphologies are observed.[365] A strong field favors the formation of columns as the evolution is dominated by the electrostatically amplified surface waves.[365,366] In contrast, a week filed allows dewetting of the top layer before the onset of electrostatic instability.[365,377,378] Temporal modulation of the electric field also significantly influences the final pattern morphology. The onset of instability is with

the formation of PS columns in a PS–PMMA bilayer, if the electric filed is applied ahead of softening of the film.[366] The columns deform the bottom PMMA layer at the film–film–air contact line and induces a secondary instability which engenders flow of PMMA around the periphery of the pre-existing PS columns, eventually resulting in an array of ordered columns with core – shell morphology (figure 9A).[366] On the other hand, if the film is initially softened, the PS film dewets on an intact PMMA under layer initially. Subsequently, the PS droplets are stretched towards the top electrode by the electric field, forming columns.[367] The deformed PMMA meniscus shows fingering instability around each PS column. The edge of the fingers climb along the periphery of the PS columns, forming narrow strands surrounding the PS core.[367] Preferential removal of the PS core results in an unique PMMA cage (figure 9B), something that can never be obtained by any lithography.[367] In case the higher dielectric PMMA film is placed over the PS film with lower dielectric constant, the electrostatic forces acts upwards at the PMMA-air interface and downwards at the PMMA – PS interfaces, which in combination with dewetting results in a novel structures such as PS core surrounded by PMMA sheath.[368]

4.3 Electric Field Induced Patterning in Visco Elastic Thin Films

EHD instability is also observed in visco elastic and purely elastic thin films.[374–381] Similar to EC instability, EHD instability in an elastic thin film has been investigated in both peel configuration,[377,378] and parallel electrode geometry.[374,375,380,381] In the first case, depending on the stiffness of the film, three distinct types of shape change along the contact zone is observed upon application of the electric field. In stiffer films, the applied field appreciably decreases the amplitude ($\boldsymbol{a_F}$) of the initial finger patterns above a critical voltage ($\mathbf{V_C}$), resulting in a nearly flat, featureless edge at higher voltages (inset of figure 10A2).

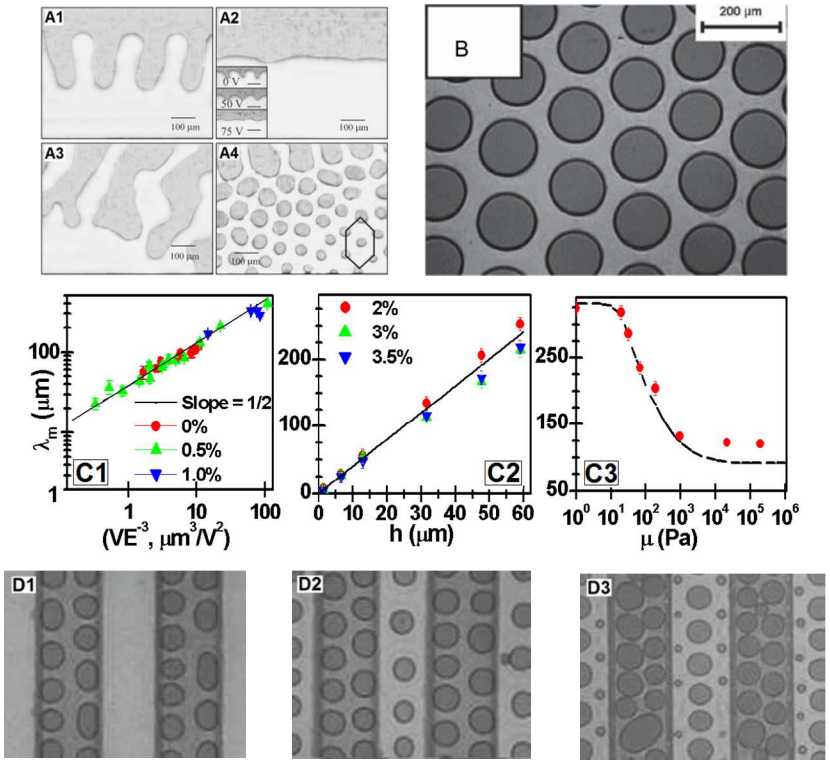

Figure 10: (A) Electric filed induced instability in a soft elastic film with a flexible contactor. (A1) Finger patterns in absence of electric field (shear modulus μ = 3.9 MPa and h =37.2 μm); (A2) "Edge straightening" in a high stiffness film with μ = 6.9 MPa and h =76.8 μm; (A3) "Finger Elongation" in a intermediate stiffness film with μ = 3.9 MPa and h =37.2 μm and (A4) "Pillar Formation" in a low stiffness film with μ = 2.2 MPa and h =29.9 μm under applied electric filed respectively. The inset in (A2) shows the "Edge straightening" sequence with increase in applied voltage. Reproduced with permission from ref. 377. Copyright 2006 WILEY-VCH Verlag GmbH & Co. (B) Typical hhexagonally ordered circular columns formed in a viscoelastic liquid PDMS film with 2% CL concentration, and V = 30 V. Reproduced with permission from ref. 381. Copyright 2011 WILEY-VCH Verlag GmbH & Co. (C1) Wavelength, λ vs VE A^{-3} in log-log scale for viscoelastic liquid like films having 0% < CL < 1%, 2.5 μm < h < 75 μm and gap spacing d varying between 30 nm and 40 μm under applied voltage between 5 V and 150 V. The line represents the viscous film theory for γ = 19:8 mN/m and ε_P = 2.65. (C2) λ as a function of h in solidlike viscoelastic films for having different CL concentrations. The line represents the best fit having a slope ~ 4.1. (C3) Transition in λ between the liquid like and the solid like as a function of elastic shear modulus. For the plot, h = 31.5 μm, V = 30 V and d = 50 μm. Reproduced with permission from ref. 380. Copyright 2009, American Physical Society. (D) Effect of temporal modulation of electric filed on a elastic film with a patterned contactor. Film thickness is μm and a top electrode stripe width w = 120 μm. (D1) An array of doublet-columns when electric field bias is 40 V (w ~ 2λ). (D2) Appearance of columns under grooves of the top electrode when the electric field is ramped up to 65 V for 2 minutes and (D3) shows the emergence of ordered thinner columns at the grooves of the patterned electrode as voltage bias is further increased to 130 V. (B and C) Reproduced with permission from ref. 381. Copyright 2011 WILEY-VCH Verlag GmbH & Co.

In films with intermediate stiffness, a rapid increase in a_F takes place beyond V_C, with concurrent multiple scissions at the elongated fingers tips (figure 10A3). In contrast, in films with even lower stiffness, the fingers break down into array of pillars (figure 10A4).[377,378] The fingers reappear upon switching off the electric field in the first case, due to a purely elastic

nature of the film. In contrast the morphological changes are permanent in the latter two cases due to enhanced viscous dissipation from the film.[377,378]

In the parallel electrode configuration, an array of columns with hexagonal closed packing is observed upon application of the electric field (figure 10B),[380,381] the morphology of which is similar to that observed in a purely viscous film.[347] In films with lower levels of elasticity, there is no $\mathbf{V_C}$ and in this regime, $\boldsymbol{\lambda}$ varies rather strongly with the visco elasticity of the film (figure 10C1).[380] In contrast, in stiffer films, instability sets in only when the applied voltage exceeds a critical $\mathbf{V_C}$. In such films, $\boldsymbol{\lambda}$ does not depend on the precise rheology of the film and exhibits a nearly linear scaling $\boldsymbol{\lambda} \approx 4\boldsymbol{h}$ with film thickness (figure 10C2). Figure 10C3 shows a clear transition of $\boldsymbol{\lambda}$ from long wave in a purely viscous film to short wave in a purely elastic films, over a narrow range of elastic modulus.[380] Pattader et al. showed that temporal modulation of the applied electric filed also influences the pattern morphology in visco elastic films, due to the appearance of secondary and tertiary structures, resulting in hierarchical patterns, which can be observed in figure 10D.[381]

4.4 Thermal Gradient Induced Patterning

A thermal gradient applied across a film can also destabilize it, resulting in meso scale features.[393–400] The experimental arrangement is nearly identical to that used in LISA, except in this case the contactor and the film is maintained at two distinct temperatures. Rearrangement of a flat film into columns spanning the two plates maximizes the heat flux, which is also associated with maximization of the rate of entropy increase. It is important to highlight that thought a temperature gradient exists, neither Rayleigh – Benrad or Benard – Marangoni convection effects are strong in case of a thin polymer film with high viscosity.

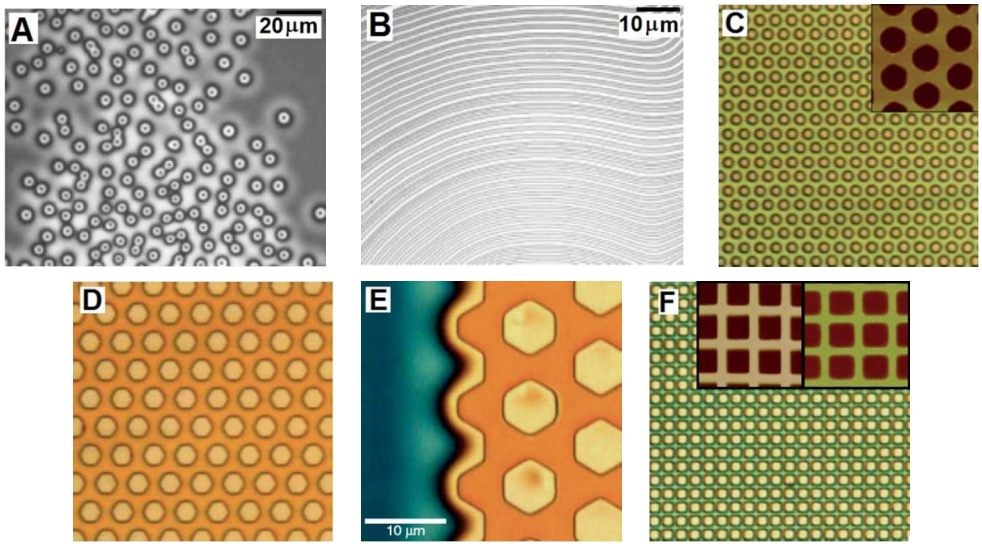

Figure 11: (A, B) Instability structures in polymer films exposed to laterally homogeneous temperature gradients by sandwiching between two flat plates at different temperature. (A) Columnar structure in a 106 nm thick PS film, gap between plates (d) = 448 nm, plate temperatures 170^{O}C (T_1) and 124^{O}C (T_2) respectively; (B) Stripe patterns in a 100 nm thick film with d = 202 nm, T_1 = 170^{O}C and T_2 = 133^{O}C. (C – E) Pattern replication in temperature-gradient driven capillary instability with a patterned top plate on the surface of a 106 nm thick PS film with variable plate spacing (d=160 nm in (C) to d= 220 nm in (E)), due to which the replicated hexagonal arrays have periodicity of 2 µm, 4 µm and 10 µm respectively. (F) Shows 500 nm cross hatched pattern. AFM images in the insets show the structure of the master and the replicated pattern respectively. Reproduced with permission from ref. 393. Copyright 2003 Wiley–VCH.

Rather, heat transfer across the polymer film with air gap is attributed to a diffusive mechanism, with molecular vibration being responsible for the transport of heat within the polymer film.[382] Depending on the fill factor ***f*** either columnar (lower ***f***, figure 11A) or striped morphology (higher f, figure 11B) is obtained.[383] The patterns can further be aligned with a topographically patterned top plate, examples of which are shown in different frames of figure 11C–F.[382]

4.5 Perspective on External Field Mediated Instability

The key advantage of EHD instability in patterning lies in it's ability to create ordered structures with a flat, featureless stamp as well as its rather material invariant nature. Scientifically this phenomena is extremely fascinating and often in conjugation with dewetting, is capable of extremely novel structures such as cages which can be ideal candidates for drug release and other nano bio technology applications. However, the experiential procedure is complicated, and reproducibility is certainly an issue. This is in fact a reason why unlike dewetting, which has

been experimented by a large number of groups worldwide, publications on EHD instability still comes only from a selected few groups. Steiner has explored and already reported most of the relevant features of EHD in a viscous film. However issues related to EHD instability in Elastic and VE films is yet to be understood fully. For example, it is seen that the columns remain intact even after switching off the electric field in an Elastic Film. However, in EC instability, the structures fade away once the contactor is withdrawn. Despite the physical cross linking of the polymer chains in the film, what precisely allows the columns to remain stuck to the top electrode is an unresolved scientific issue. Even in a viscous film, whether the presence of conducting nano particles in trace quantity will influence the instability or not can be another fascinating problem. One may take clue from EHD experiments and can see the effect of an external magnetic field in polymer films containing magnetic nano particles.

5.0 Conclusions and Perspective:

The review presented here provides an illustrative commentary about the progress and recent developments on the rich phenomenon of surface instability and morphological evolution of an incompressible visco elastic thin film. The key emphasis of the review has been to discuss the conditions under which instability mediated structures can be ordered, often in conjugation with some top down lithography method, for possible fabrication of novel structures spanning over large areas that are difficult to realize with conventional top down techniques. We have discussed how historically research on meso-mechanics of polymer thin films has progressed following three distinct routes, depending on the nature of the confining field and to some extent, the rheology of the film. To facilitate discussion, we have categorized the instabilities in three distinct regimes. At this point we would like to highlight the fundamental difference between spontaneous instability (category 1) with both contact proximity induced (category 2) and

external field mediated (category 3) instabilities. In the first case, the morphological evolution is associated with lowering of the free energy of the system. In contrast, when an external field is applied, the system is intrinsically out of equilibrium and an exact equivalent of the Gibbs' free energy is difficult to formulate. Consequently, the morphological evolution in the latter case is associated with the maximization of the flux.[389]

At this point we would like to highlight a relatively new formulation by Sarkar and Sharma, where based on linear stability analysis it is argued that these apparently distinct categories of instabilities are manifestation of generic instability in a soft visco elastic thin film.[314] It is seen that the nature of the instability (shortwave or long-wave) of a viscoelastic films, in both the wetting and adhesive configurations, is determined by a parameter $\boldsymbol{\gamma/\mu h}$. One limiting case is a confined a purely elastic film, for which $\boldsymbol{\gamma/\mu h}$ is $<10^{-2}$, which corresponds to $\mathbf{h_{km}}$=2.12 and λ = 2.96**h**, On the other extreme, in a purely viscous wetting film $\boldsymbol{\gamma/\mu h}$ is >1 and the critical wavelength acquires a long-wave nature.[314] A gradual transition of the nature of the instability length scale from long wave to short wave with enhanced visco elasticity has been nicely captured by Arun et al.[391] in the context of EHD of a visco elastic thin film. It strengthens this arguement of visualizing the apparently different settings as different limiting cases of a generic instability in soft visco elastic thin films. It is clearly seen that progress in this field has been made based on combination of robust theoretical modeling and simulations, along with carefully performed experiments. Simulations greatly reduce the experimental efforts, and nicely capture regime cross overs which are difficult to obtain based on pure experiments.

We have added a perspective for each theme which highlights some of the yet resolved issues for each theme, and have specifically mentioned the practical utility of instability mediated fabrication in nano patterning. This review adequately highlights the advantages of instability

mediated patterning, in terms of richness of physics as well as the flexibility the methods offer in terms of morphology control, which allows possible fabrication of various different structures and are not mere negative replica of stamp features as well as their in situ modulation based on controlling the initial conditions. However, delicate experimental protocols and sensitivity towards initial conditions, bulk nano fabrication of instability mediated structures might take some time before it reaches the level of commercialization, particularly for implementation of beyond the master patterning concepts.[397–399]

We would like to remind the readers that instability in a thin film is observed in many other settings, but in order to keep the review focused, only instability observed with homo polymer thin films are discussed in this article. Many examples that involve phase segregation like polymer blends, block co polymers, evaporation induced assemblies are not included. As a final summary, instability mediated patterning indeed seems a promising approach for fabrication of novel meso and nano structures in a rapid, cost effective manner. Future progress in this area will involve structure formation in functional polymers with more complicated molecular architecture and their potential integration into devices such as sensors, solar cells, bio chips etc. to name a few.

References:

1. L. H. Sperling (1997). *Polymeric Multicomponent Materials: an Introduction to LED.* New York, NY: Wiley Interscience.
2. R. Duncan. *Nature Rev./Drug Discovery* 2003, **2**, 347.
3. B. D. Gates, Q. Xu, M. Stewart, D. Ryan, C. G. Willson and G. M. Whitesides, *Chem. Rev.*, 2005, **105**, 1171.
4. N. Francesco, B. Francesco, C. Donato, M. Gianluca, Q. Fabio, R. Roberto, T. Raffaele and V. Ludovico, *J. Am. Chem. Soc.*, 2003, *125*, 9055.
5. Stone, H. A., and S. Kim, *AIChE J.*, 2011, **47**, 1250.
6. Z. W. Wicks Jr., F. N. Jones, S. P. Pappas and D. A. Wicks (2007) *Organic Coatings: Science and Technology*, 3rd Edition, Hoboken, NJ. John Wiley & Sons, Inc.
7. R. K. Jain, I. Ivanov, C. Maldarelli and E. Ruckenstein (1978), Instability and Rupture of Thin Liquid Films. in T. S. Sorensen (ed.) *Dynamics and Instability of Fluid Interfaces*. Berlin Heidelberg: Springer–Verlag.
8. R. Mukherjee, A. Sharma and U. Steiner. (2011) *Surface Instability and Pattern Formation in Thin Polymer Films*. in A. del Campo and E. Artz (Eds.), *Generating Micro- and Nanopatterns on Polymeric Materials,* Weinheim: WILEY–VCH Verlag & Co. KgaA. (pp. 217–265).
9. G. M. Whitesides, J. P. Mathias and C. T. Seto, *Science,* 1991, **254**, 1312.
10. G. A. Ozin and A. C. Arsenault (2005), *Nanochemistry*: *A Chemical Approach to Nano Materials.* Cambridge, Royal Society of Chemistry.
11. L. D. Landau and E. M. Lifshitz, (1960) *Electrodynamics of Continuous Media*, Oxford, Pergamon Press.
12. I. E. Dzyaloshinskii, E.M. Lifshitz and L. P. Pitaevskii, *Adv. Phys*., 1961, **10**, 165.
13. J. W. Cahn, *J. Chem. Phys.*, 1965, **42**, 93.
14. A. Vrij Discuss. *Faraday Soc*., 1066, **42**, 23.
15. A. Vrij and J. Overbeek, *Am. Chem. Soc*., 1968, **90**, 3074.
16. R. K. Jain and E. Ruckenstein, *J. Colloid Interf. Sci*., 1976, **54**, 108.
17. M. B. Williams and S. H. Davis, *J. Coll. Interf. Sci.,* 1982, **90**, 220.
18. A. Sharma and E. Ruckenstein, *J. Colloid Interf*., Sci., 1985, **106**, 12.
19. P. G. de Gennes, *Rev. Mod. Phys.,* 1985, **57**, 827.
20. C. J. Van Oss, M. K Chaudhury and R. J. Good, *Chem. Rev*., 1988, **88**, 927.
21. B. V. Derjaguin, *Theory of Stability of Thin Films and Colloids*, 1989.
22. A. Sharma and E. Ruckenstein, *J. Colloid Interf. Sci*., 1990, **137**, 433.
23. F. Brochard-Wyart, J. M. di Meglio and D. Qu´er´e, P. G. deGennes, *Langmuir,* 1991, **7**, 335.
24. J. Israelchvili (2011) *Intermolecular and Surface Forces, Third Edition,* Academic Press, Elsavier.
25. A. Sharma, *Langmuir*, 1993, **9**, 861.
26. M. P. Ida and M. J. Miksis, *Appl. Math. Lett., 1996,* **9**, 35.

27. P. G. de Gennes, F. Brochard-Wyart and D. Quere´ (2004). *Capillarity and Wetting Phenomena: Drops, Bubbles, Pearls, Waves*. London, Springer.
28. X. – M. Li, D. Reinhoudt and M. Crego-Calama, *Chem Soc. Rev.* 2007, **36**, 1350.
29. J. Sun, B. Bhushan and J. Tong, *RSC Advances* 2013, **3**, 14862.
30. X. Liu, Y. Liang, F.Zhou and W. Liu, *Soft Matter*, 2012, **8**, 2070.
31. G. Krausch, *Mater. Sci Engg. Reports*, 1995, **14**, 1.
32. G. Krausch, *J Phys: Condens Matter.,* 1997, **9**, 7741.
33. A. Oron, S. H. Davis and S. G. Bankoff, *Rev. Mod. Phys.,* 1997, **69**, 931.
34. R. A. L Jones, *Curr. Opin. Coll. Interf. Sci.,* 1999, **4**, 153.
35. P. Müller-Buschbaum, *J. Phys Cond. Matter.,* 2003, **15**, R1549.
36. M. Geoghegan and G. Krausch, *Prog. Polym. Sci.*, 2003, **28**, 261
37. D. G. Bucknall, *Prog. Mater. Sci.,* 2004, **49**, 713.
38. P. Müller-Buschbaum, E. Bauer, O. Wunnicke and M. Stamm, *J. Phys.: Condens. Matter,* 2005, **17**, S363.
39. S. Kalliadasis and U. Thiele (2007). *Thin Films of Soft Matter*. New York, NY: SpringerWien
40. K. Jacobs, S. Herminghaus and R. Seemann. (2008) *Stability and Dewetting of Thin Liquid Films*, in O. K. C. Tsui and T. Russel (eds.), *Thin Liquid Films*, Singapore: World Scientific Review. (pp 243–265)
41. O. K. C. Tsui. (2008) *Anomalous Dynamics of Polymer Films*, in O. K. C. Tsui and T. Russel (eds.), *Thin Liquid Films*, Singapore: World Scientific Review. (pp 267–294)
42. A. del Campo and Eduard Arzt, *Chem. Rev.*, 2008, **108**, 911.
43. R. V. Craster and O. K. Matar, *Rev. Mod. Phys.*, 2009, **81**, 1131.
44. R. Mukherjee (2011) *Liquid Thin Film Hydrodynamics: Dewetting and Pattern Formation*. in S. Chakraborty (ed.), *Mechanics over Micro and Nano Scales,* New York, NY: Springer. (pp. 193–215).
45. M. Ramanathan and S. B. Darling, *Prog. Polym. Sci*., 2011, **36**, 793.
46. L. Xue and Y. Han, *Prog. Polym. Sci.*, 2011, **36**, 269.
47. D. Gentili, G. Foschi, F. Valle, M. Vavallini and F. Biscarini, *Chem Soc. Rev.*, 2012, **41**, 4430.
48. A. Sharma and E. Ruckenstein, *J. Colloid Interface Sci.,* 1985, **111**, 8.
49. A. Sharma and E. Ruckenstein, *Langmuir,* 1986, **2**, 480.
50. A. Sharma, *J. Dispersion Sci. Technol.,* 1992, **13**, 459.
51. A. Sharma and R. Khanna, *J. Chem. Phys.,* 1999, **110**, 4929.
52. R. Fondecave and F. Brochard -Wyart , *Macromolecules*, 1998, **31**, 9305
53. F. Brochad -Wyart and J. Daillant, *Can. J. Phys.*, 1990, **68**, 1084.
54. V. S. Mitlin, *J. Coll. Interf. Sci.*, 1993, **156**, 491.
55. V. S. Mitlin and M. M. Sharma, *J. Coll. Interf. Sci.,* 1993, **157**, 447.
56. V. S. Mitlin, *Coll. Surf. A.*, 1994, **89**, 97.
57. V.S. Mitlin, *J. Coll. Interf. Sci.*, 1995, **170**, 65.
58. A. Sharma and A. T. Jameel, *J. Coll. Interf. Sci.,* 1993, **161**, 190.
59. A. Sharma and A. T. Jameel, *J. Chem. Soc. Faraday Trans.*, 1994, **90**, 625.

60. R. Khanna, A. T. Jameel and A. Sharma, *Ind. Engg. Chem. Res.*, 1996, **35**, 3081.
61. R. Khanna and A. Sharma, *J. Colloid Interf. Sci.,* 1997, **195**, 42.
62. A. Ghatak, R. Khanna and A. Sharma, *J. Colloid Interf. Sci.*, 1999, **212**, 483.
63. A. Sharma, R. Khanna and G. Reiter, *Colloids Surf. B*, 1999, **14**, 223.
64. A. Oron and S. G. Bankoff, *J. Colloid Interf. Sci.*, 1999, **218**, 152.
65. M. Müller, L. G .MacDowell, P. Müller-Buschbaum, O. Wunnicke and M. Stamm, *J. Chem. Phys.,* 2001, **115**, 9960.
66. A. M. Leshansky and B. Y. Rubinstein, *Phys. Rev.*, 2005, E **71**, 040601(R).
67. J. Becker and G. Grun, *J. Phys.: Condens. Matter 17*, 2005, S291
68. H. Zhao, O. K.C. Tsui and Z. Liu, *Solid State Comm.*, 2005, **134**, 455.
69. O. Pierre-Louis, A. Chame and Y. Saito, *Phys. Rev. Lett.,* 2009, **103**, 195501.
70. A. Sharma and R. Khanna, *Phys. Rev. Lett.,* 1998, **81**, 3463.
71. A. Oron, *Phys. Rev. Lett.*, 2000, **85**, 2108.
72. A. Sharma, *Euro Phys J E*, 2003, **12**, 397.
73. R. Verma and A. Sharma, *Ind. Engg. Chem. Res.*, 2007, **46**, 3108.
74. A. Sharma and R. Verma, *Langmuir*, 2004, **20**, 10337.
75. H. Zhao, Y. J. Wang and O. K. C. Tsui, *Langmuir,* 2005, **21**, 5817.
76. C. Redon, F. Brochad -Wyart and F. Rondelez, *Phys. Rev. Lett*., 1991, **66**, 715.
77. G. Reiter, *Phys. Rev Lett.,* 1992, **68**, 75.
78. G. Reiter, *Langmuir,* 1993, **9**, 1344.
79. G. Reiter, *Macromolecules*, 1994, **27**, 3046.
80. W. Zhao, M. H. Rafailovich, J. Sokolov, L.J. Fetters, R. Plano, M. K. Sanyal, S. K. Sinha and B. B. Sauer. *Phys Rev Lett*., 1993, **70**, 1453.
81. K. R. Shull and T. E. Karis, *Langmuir*, 1994, **10**, 334.
82. A. Sharma and G. Reiter, *J. Colloid Interf. Sci*., 1996, **178**, 383.
83. R. Xie, A. Karim, J. F. Douglas, C. C. Han and R. A. Weiss, *Phys. Rev. Lett.,* 1998, **81**, 1251.
84. H. I. Kim, C. M. Mate, K. A. Hannibal and S. S. Perry, Phys. Rev. Lett. 82, 3496, 1999.
85. M. O. David, G. Reiter, T. Sitthai, and J. Schultz, *Langmuir*, 1998, **14**, 5667.
86. A. Martin, O. Rossier, A. Buguin, P. Auroy and F. Brochad -Wyart, *Eur Phys J E,* 2000, **3**, 337.
87. G. Reiter, R. Khanna and A. Sharma, *Phys. Rev. Lett.,* 2000, **85**, 1432.
88. G. Reiter, A. Sharma, R. Khanna, A. Casoli and M. O. David, *J. Colloid Interf. Sci.*, 1999, **214**, 126.
89. A. Sharma and G. Reiter, *Phase Trans*., 2002, **75**, 377.
90. R. Mukherjee, D. Bandyopadhyay and A. Sharma, *Soft Matter*, 2008, **4**, 2086.
91. Elbaum, M., and S. G. Lipson, 1994, *Phys. Rev. Lett*., 1994, **72**, 3562.
92. A. Sharma, *Langmuir*, 1998, **14**, 4915.
93. U. Thiele, M. Mertig and W. Pompe. *Phys Rev Lett*., 1998, **80**, 2869.
94. P. Martin and F. Brochard-Wyart, *Phys Rev Lett*., 1998, **80**, 3296.

95. K. Jacobs, S. Herminghaus and K. R. Mecke, *Langmuir,* 1998, **14**, 965.
96. M. Sferrazza, M. Heppenstallbutler, R. Cubitt, D. G. Bucknall, J. Webster and R. A. L. Jones, *Phys. Rev. Lett.*, 1998, **81**, 5173.
97. J. C. Meredith, A. P. Smith, A. Karim and E. J. Amis, *Macromolecules*, 2000, **33**, 9747.
98. R. Konnur, K. Kargupta and A. Sharma, *Phys. Rev. Lett.*, 2000, **84**, 931.
99. M. Zope, K. Kargupta and A. Sharma, *J. Chem. Phys.*, 2001, **114**, 7211.
100. K. Kargupta, R. Konnur and A. Sharma, *Langmuir*, 2001, **17**, 1294.
101. U. Thiele, M. G. Velarde and K. Neuffer, *Phys. Rev. Lett*., 2001, **87**, 016104.
102. R. Seemann, S. Herminghaus and K. Jacobs, *Phys. Rev. Lett.*, 2001, **86**, 5534.
103. R. Seemann, K. Jacobs and R. Blossey, *J. Phys.: Condens. Matter*, 2001, **13**, 4915.
104. R Seemann, S Herminghaus and K Jacobs, *J. Phys.: Condens. Matter,* 2001, 13, 4925.
105. Martin A, Buguin A, and Brochard-Wyart F, *Langmuir,* 2001, 17, 6553.
106. I. Karapanagiotis, D. Fennell Evans and W. W. Gerberich, *Macromolecules,* 2001, **34**, 3741.
107. I. Karapanagiotis, D. Fennell Evans and W. W. Gerberich, *Langmuir*, 2001, **17**, 3266.
108. K. Kargupta and A. Sharma, *J. Coll. Interf. Sci*., 2002, **245**, 99.
109. Karapanagiotis, D. F. Evans and W. W. Gerberich, *Colloids Surf. A,* 2002, **207**, 59.
110. B. Du, F. Xie, Y. Wang, Z. Yang and O. K. C. Tsui, *Langmuir,* 2002, **18**, 8510.
111. L. Brusch, H. Kühne, U. Thiele and M. Bär, *Phys. Rev. E,*2002, **66**, 011602.
112. K. M. Ashley, J. C. Meredith, E. Amis, D. Raghavan and A. Karim, *Polymer,* 2003, **44**, 769.
113. C. Neto, K. Jacobs, R. Seemann, R. Blossey, J. Becker and G. Grün, *J. Phys*.: *Condens. Matter,* 2003, **15**, S421.
114. C. Neto, K. Jacobs, R. Seemann, R. Blossey, J. Becker and G. Grün, *J. Phys.: Condens. Matter,* 2003, **15**, 3355.
115. J. Becker, G. Grün, R. Seeman, H. Mantz, K. Jacobs, K. R. Mecke and R. Blossey, *Nat. Mater,* 2003, **2**, 59.
116. I. Karapanageotis and W. W. Gerberich, *Surf. Sci*., 2005, **594***,* 192.
117. I. Karapanageotis and W. W. Gerberich, *Langmuir,* 2005, **21**, 9194.
118. Y. J. Wang and O. K. C. Tsui, *Langmuir*, 2006, **22**, 1959.
119. E. Bauer, E. Maurer, T. Mehaddene, S. V. Roth and P. Muller-Buschbaum, *Macromolecules,* 2006, **39**, 5087.
120. C. Renger, P. Müller-Buschbaum, M. Stamm, and G. Hinrichsen, *Macromolecules,*2000, **33***,* 8388.
121. O. Baumchen, J. D. McGraw, J. A. Forrest and K. Dalnoki-Veress *Phys Rev. Lett*., 2012, **109**, 055701.
122. H. S. Jeon, P. S. Dixit and H. Yim, *J. Chem. Phys.,*2005, **122**, 104707.
123. O. K. Matar, V. Gkanis and S. Kumar, *J. Colloid Interf. Sci,* 2005, **286**, 319.
124. A. Faldi, R. J. Composto and K. I. Winey, *Langmuir,* 1998, **11***,* 4855.
125. S. Sheiko, E. Lermann, and M. Moller, *Langmuir,* 1996, **12**, 4015.
126. Dongzhong Chen, Hitesh Handa, Lei Wan, Guangzhao Mao, *Macromol. Rapid Commun*. 2007, **28**, 1619.

127. S. Herminghaus, A. Fery, S. Schlagowski, K. Jacobs, R. Seemann, H. Gau, W. Monch and T. Pompe, *J. Phys.: Condens. Matter,*2000, 12, A57.
128. S. Herminghaus, K. Jacobs, K. Mecke, J. Bischof, A. Fery, M. Ibn-Elhaj and S. Schlagowski, *Science,* 1998, 282, 916.
129. A.L. Demirel and B. Jerome, *Europhys. Lett.* 1999, 45, 58.
130. B. Ravi, R. Mukherjee and D. Bandyopadhyay, *Soft Matter* 2015, 11, 139.
131. M. W. J. van der Wielen, M. A. Cohen Stuart, and G. J. Fleer, *Langmuir* 1998, 14 7065.
132. K. Fukuzawa, T. Yoshida, S. Itoh and H. Zhang, *Langmuir* 2008, 24, 11645.
133. Brochard-Wyart F, and Redon C, *Langmuir,* 1992, 8*,* 2324.
134. A Munch, *J. Phys.: Condens. Matter,* 2005, 17, S309.
135. S.-H. Choi and B.-M. Zhang Newby, *J. Chem. Phys.,* 2006, 124, 054702.
136. B. M. Besancon and P. F. Green, *Phys. Rev. E,* 2004, 70, 051808.
137. M. Oron, T. Kerle, R. Yarushalmi-Rozen and J. Klein, *Phys. Rev. Lett*., 2004 92, 236104.
138. I. Leizerson, S. G. Lipson and A. V. Lyushnin, *Langmuir,* 2004, *20*, 291.
139. S. Gabriele, S. Sclavons, G. Reiter and P. Damman, *Phys. Rev. Lett.,* 2005, 96, 156105.
140. P. Muller-Buschbaum, J. S. Gutmann and M. Stamm, *Phys Chem* 1, 1999, 3857.
141. E. Bonaccurso, H.-J. Butt, V. Franz, K. Graf, M. Kappl, S. Loi, B. Niesenhaus, S. Chemnitz, M. Bohm, B. Petrova, U. Jonas and H. W. Spiess, 2002, 18*,* 8056.
142. S. H. Lee, P. J. Yoo, S. J. Kwo and H. H. Lee, *J. Chem. Phys.*,2004, **121**, 4346.
143. L. Xu, T. Shi, and L. An, *Langmuir*, 2007, 23, 9282.
144. L. Xue, Y. Han, *Langmuir*,2009, 25, 5135.
145. X. Chen and M. Anthamatten, *Langmuir* ,2009, 25*,* 11555.
146. J. –L. Masson and P. F. Green, *Phys. Rev. Lett.,* 2002, 88, 205504.
147. R. Limary and P. F. Green, *Langmuir,*2003, 19, 2419.
148. K. B. Glasner and T. P. Witelski, *Phys. Rev. E ,* 2003, 67, 016302.
149. A. Verma and A. Sharma, *Adv. Mater.,* 2010, 22, 5306.
150. A. Verma and A. Sharma, *Macromolecules,* 2011, 44, 4928.
151. A. Verma and A. Sharma, *Soft Matter*, 2012.
152. O. K. C. Tsui, Y. J. Wang, H. Zhao and B. Du, *Euro Phys J E,* 2003, **12**, 417.
153. U. Thiele, *Euro Phys. J E,* 2003, **12**, 409.
154. H. Kaya and B. Jerome*, EPJE,* 2003, **12**, 383.
155. P. F. Green and V. Ganesan, *Euro Phys. J E*, 2003, 12**,** 449.
156. H. Richardson, C. Carelli, J. K. Keddie and M. Sferrazza, *Euro Phys. J E*, 2003, 12, 437.
157. C. Bollinne, S. Cuenot, B. Nysten and A. M. Jonas, *Euro Phys. J. E ,* 2003, **12**, 389.
158. A. Sharma and J. Mittal, *Phys. Rev. Lett*., 2002, **89**, 186101.
159. K. D. F. Wensink,and B. Jerome, *Langmuir*, 2002, **18**, 413.
160. M. D. Morariu, E. Schäffer and U. Steiner, *Phys. Rev. Lett.,* 2004, **92**, 156102.

161. R. Fetzer, M. Rauscher, R. Seemann, K. Jacobs, and K. Mecke, *Phys Rev. Lett*.,2007, **99**, 114503.
162. M. H. Yang, S. Y. Hou, Y. L. Chang, A. M. Yang, *Phys. Rev. Lett*., 2006, **96**, 066105.
163. G. Henn, D. G. Bucknall, M. Stamm, P. Vanhoorne and R. Jerome, *Macromolecules,* 1996, **29**, 4305.
164. P. Müller-Buschbaum and M. Stamm, *Macromolecules*,1998, **31**, 3686.
165. P. Müller Buschbaum, *Euro Phys J E* , 2003, **12**, 443.
166. G. Reiter and P.-G. de Gennes, *Eur. Phys. J. E*, 2001, **6**, 25 .
167. H. Bodiguel and C. Fretigny, *Eur. Phys. J. E,* 2006, **19**, 185.
168. G. Reiter, M. Hamieh, P. Damman, S. Sclavons, S. Gabriele, T. Vilmin and E. Raphaël, *Nat Mater.,* 2005, **4**, 754.
169. F. Brochard, and P. G. de Gennes, *Langmuir,* 1992, **8**, 3033.
170. F. Brochard, P. G. de Gennes, H. Hervert and C. Redon, *Langmuir,* 1994, **10**, 1566.
171. C. Redon, J. B. Brzoska and F. Brochard-Wyart, *Macromolecules*, 1994, **27**, 468.
172. A. Sharma and R. Khanna, *Macromolecules*, 1996, **29**, 6959.
173. F. Brochard-Wyart, G. Debregeas, R. Fondecave, and P. Martin, *Macromolecules*, 1997, **30**, 1211.
174. T. G. Stange, D. F. Evans and W. A. Hendrickson, *Langmuir*, 1997, **13**, 4459.
175. K. Jacobs, R. Seemann, G. Schatz and S. Herminghaus, *Langmuir*, 1998, **14**, 4961.
176. Dalnoki-Veress K., Nickel B. G., Roth C. and Dutcher J. R., *Phys. Rev. E*, 1999, **59**, 2153.
177. G. Reiter, *Phys. Rev. Lett*. , 2001, **87**, 186101.
178. N. Alleborn, A. Sharma and A. Delgado, *Can J Chem Engg*., 2007, **85**, 586.
179. R. Seemann, S. Herminghaus and K. Jacobs*, Phys. Rev. Lett*. , 2001, **87**, 196101.
180. F. Saulnier, E. Raphaël and P.-G. de Gennes, *Phys. Rev. Lett*., 2001, **88**, 196101.
181. F. Saulnier, E. Raphaël and P.-G. de Gennes, *Phys. Rev. E*., 2002, **66**, 061607.
182. Martin A, Clain J, Buguin A, and Brochard-Wyart F., Phys *Rev E*, 2002, **65**, 031605.
183. V. Shenoy and A. Sharma, *Phys. Rev. Lett.,* 2002, **88**, 236101.
184. S. Herminghaus, R. Seemann and K. Jacobs, *Phys. Rev. Letts*., 2002, **89**, 056101.
185. A. Sharma and K. Kargupta, *Appl. Phys. Lett.,* 2003, **83**, 3549.
186. P. Damman, N. Baudelet and G. Reiter, *Phys. Rev. Lett*., 2003, **91**, 216101.
187. S. Herminghaus, K. Jacobs and R. Seemann, *Eur. Phys. J. E*, 2003, **12**, 101.
188. K. Kargupta, A. Sharma and R. Khanna, *Langmuir,* 2004, **20**, 244.
189. R. Seemann, S. Herminghaus, C. Neto, S. Schlagowski, D. Podzimek, R. Konrad, H. Mantz and K. Jacobs, *J. Phys.: Condens. Matter*, 2005, **17**, S267.
190. T. Vilmin and E. Raphael, *Europhys. Lett*., 2005, **72**, 781.
191. G. Reiter, M. Sferrazza, and P. Damman, *Eur. Phys J E*, 2003, **12**, 133.
192. R. Fetzer, K. Jacobs, A. Munch, B. Wagner and T. P. Witelski, *Phys. Rev. Lett.* , 2005, **95**, 127801.
193. R. Fetzer, M. Rauscher, A. Münch, B. A. Wagner and K. Jacobs, *Europhys. Lett.,* 2006, **75**, 638.
194. T. Vilmin and E. Raphaël, *Phys. Rev. Lett*., 2006, **97**, 036105.

195. S. Gabriele, P. Damman, S. Sclavons, S. Desprez, S. Coppee, G. Reiter, M. Hamieh, S. Al Akhrass, T. Vilmin and E. Raphael, *J. Polym. Sci. B*, 2006, **44**, 3022.

196. T. Vilmin, E. Raphael, P. Damman, S. Sclavons, S. Gabriele, M. Hamieh and G. Reiter, *Europhys. Lett.*, 2006, **73**, 906.

197. T. Vilmin and E. Raphaël, *Eur. Phys. J. E*, 2006, **21**, 161.

198. R. Fetzer, and K. Jacobs, *Langmuir*, 2007, **23**, 11617.

199. P. Damman, S. Gabriele, S. Coppée, S. Desprez, D. Villers, T. Vilmin, E. Raphaël, M. Hamieh, S. Al Akhrass, and G. Reiter, *Phys. Rev. Lett.*,2007, **99**, 036101.

200. M. Hamieh, S. Al Akhrass, T. Hamieh, P. Damman, S. Gabriele, T. Vilmin, E. Raphaël and G. Reiter, *J. Adhes*., 2007, **83**, 367.

201. R. Fetzer, M. Rauscher, S. Seemann, K. Jacobs and K. Mecke, *Phys. Rev. Lett*., 2007, **99**, 114503.

202. S. Al Akhrass, R. –V. Ostaci, Y. Grohens, E. Drockenmuller and G. Reiter, *Langmuir,*2008, **24**, 1884.

203. F. Ziebert and E. Raphaël, *Phys Rev E*, 2009, **79**, 031605.

204. S. Al Akhrass, G. Reiter, S.Y. Hou, M. H. Yang, Y. L. Chang, F. C. Chang, C. F. Wang, and A. C.-M. Yang, *Phys. Rev. Lett.*, 2008, **100,** 178301.

205. O. Bäumchen, R. Fetzer, and K. Jacobs, *Phys Rev. Lett.*, 2009, **103**, 247801.

206. O. Bäumchen and K. Jacobs, *J. Phys.: Condens. Matter* , 2010, **22**, 033102.

207. K. R. Shull, *Faraday Discuss.*, 1994, **98**, 203.

208. K. R. Shull, *Macromolecules*, 1996, **29**, 8487.

209. P. G. Ferreira, A. Ajdari, L. Leibler *Macromolecules*, 1998, 31, 3994.

210. G. Reiter, A. Sharma, A. Casoli, M. O. David, R. Khanna and P. Auroy, *Langmuir*, 1999, **15**, 2551.

211. G. Reiter and R. Khanna, *Langmuir*, 2000, **16**, 6351.

212. G. Reiter and A. Sharma, *Phys. Rev. Lett.*, 2001, **87**, 166103.

213. A. Voronov and O. Shafranska, *Polymer*, 2003, **44**, 277.

214. L. Xu, A. Sharma, and S. W. Joo, *Macromolecules*, 2010, **43**, 7759.

215. L. Rayleigh, *Proc. London Math. Soc.*, 1878, **10**, 4.

216. L. Rayleigh, *Philos. Mag.*, 1892, **34**, 145.

217. G. Debregeas, P. Marticn and F. Brochard-Wyart, *Phys. Rev. Lett.*, 1995, **75**, 3886.

218. G. Debregeas, P.-G. de Gennes and F. Brochard-Wyart, *Science*, 1998, **279**, 1704.

219. S.A. Safran and J. Klein, *J. Phys. II*, 1993, **3**, 749.

220. R. Mukherjee, S. Das, A. Das, S. K. Sharma, A. K. Raychaudhuri and A. Sharma, *ACS Nano*, 2010, **4**, 3709.

221. M. Higgins and R. A. L. Jones, *Nature*, 2000, **404**, 476.

222. X. Zhang, F. Xie and O. K. C. Tsui, *Polymer*, 2005, **46**, 8416.

223. P. Müller-Buschbaum, E. Bauer, E. Maurer, K. Schlögl, S. V. Roth and R. Gehrke, *Appl. Phys. Lett.*, 2006, **88**, 083114.

224. H.–G. Braun and E. Mayer, *Thin Solid Films*, 1999, **345**, 222.

225. E. Mayer and H.-G. Braun, *Macromol. Mater. Eng.*, 2000, **44**, 276.
226. M. K. Erhardt and R. G. Nuzzo, *J. Phys. Chem. B*, 2001, **105**, 8776.
227. X. Wang, M. Ostblom, T. Johansson and O. Inganas, *Thin Solid Films*, 2004, **449**, 125.
228. X. Wang, K. Tvingstedt and O. Inganas, *Nanotechnology*, 2005, **16**, 437.
229. J. Z. Wang, Z. H. Zheng, H. W. Li, W. T. S. Huck and H. Sirringhaus, *Nat. Mater.*, 2004, **3**, 171.
230. M. Cavallini, M. Facchini, M. Massi, and F. Biscarini, *Synth. Met.*, 2004, **146**, 283.
231. W. Li, Y. Nie, J. Zhang, D. Zhu, X. Li, H. Sun, K. Yu and B. Yang, *Macromol. Chem. Phys.* 2008, **209**, 247.
232. G. Lu, W. Li, J. Yao, G, Zhang, B. Yang and J. Shen, *Adv. Mater.*, 2002, **14**, 1049.
233. A. Sehgal, V. Ferreiro, J. F. Douglas, E. J. Amis and A. Karim, *Langmuir*, 2002, **18**, 7041.
234. Z. Zhang, Z. Wang, R. Xing and Y. Han, *Polymer*, 2003, **44**, 3737.
235. Z. Zhang, Z. Wang, R. Xing and Y. Han, *Surf. Sci.*, 2003, **539**, 129.
236. A. Sehgal, D. Bandyopadhyay, K. Kargupta, A. Sharma and A. Karim, *Soft Matter*, 2012, **8**, 10394.
237. D. Julthongpiput, W. Zhang, J. F. Douglas, A. Karim and M. J. Fasolka, *Soft Matter*, 2007, **3**, 613.
238. K. Kargupta and A. Sharma, *Phys. Rev. Lett.*, 2001, **86**, 4536.
239. K. Kargupta and A. Sharma *J. Chem. Phys.*, 2002, **116**, 3042.
240. K. Kargupta, R. Konnur and A. Sharma, *Langmuir*, 2000, **16**, 10243.
241. K. Kargupta and A. Sharma, *Langmuir*, 2002, **18**, 1893.
242. K. Kargupta and A. Sharma, *Langmuir*, 2003, **19**, 5153.
243. B. Suman and S. Kumar, *J. Colloid Interf. Sci.*, 2006, **304**, 208.
244. P. Volodin and A. Kondyurin, *J. Phys. D: Appl. Phys.*, 2008, **41**, 065306.
245. U. Thiele, L. Brusch, M. Bestehorn and M. Baer, *Euro Phys. J. E*, 2003, **11**, 255.
246. R. Borcia and M. Bestehorn, *Langmuir*, 2009, **25**, 1919.
247. Z. Li, M. Tolan, T. Hohr, D. Kharas, S. Qu, J. Sokolov and M. H. Rafailovich, *Macromolecules*, 1998, **31**, 1915.
248. S. Roy, K. J. Ansari, S. S. K. Jampa, P. Vutukuri and R. Mukherjee, *ACS Appl. Mater. Interfaces*, 2012, **4**, 1887.
249. N. Ferrell and D. Hansford, *Macromol. Rapid Comm.*, 2007, **28**, 966.
250. Z. Xin , B. Su , J. Wang , X. Zhang , Z. Zhang, M. Deng , Y. Song and L. Jiang, *Small*, 2013, **9**, 722.
251. N. Bhandaru, A. Das, N. Salunke and R. Mukherjee, *Nanoletts*. 2014, **14**, 7009.
252. N. Rhese, C. Wang, M. Hund, M. Geoghegan, R. Magerle and G. Krausch, *Euro Phys. J. E*, 2001, **4**, 69.
253. M. Geoghegan, C. Wang, N. Rhese, R. Magerle and G. Krausch, *J. Phys.: Condens. Matter*, 2005, **17**, S389.
254. C. Luo, R. Xing, Z. Zhang, J. Fu and Y. Han, *J. Coll. Interf. Sci.*, 2004, **269**, 158.
255. R. Mukherjee, M. Gonuguntla and A. Sharma, *J. Nanosci. Nanotechnol.*, 2007, **7**, 2069.
256. R. Xing, C. Luo, Z. Wang and Y. Han, *Polymer*, 2007, **48**, 3574.

257. K. Khare, M. Brinkmann, B. M. Law, E. L. Gurevich, S. Herminghaus and R. Seemann, *Langmuir*, 2007, **23**, 12138.
258. B. Yoon, H. Acharya, G. Lee, H. C. Kim, J. Huhc and C. Park, *Soft Matter*, 2008, **4**, 1467.
259. S. Roy and R. Mukhrejee, *ACS Appl. Mater. Interfaces*, 2012, **4**, 5375.
260. M. L. Chabinyc, W. S. Wong, A. Salleo, K. E. Paul and R. A. Street, *Appl. Phys. Lett.*, 2002, **81**, 4260.
261. N. Nhandaru, P. S. Goohpattader, D. Faruqui, R. Mukherjee and A. Sharma, *Langmuir*, 2015, **31**, 3203.
262. S. Rath, M. Heilig, H. Port and J. Wrachtrup, *Nanoletters*, 2007, **7**, 3845.
263. G. T. Lee, B. K. Yoon, H. Acharya, C. M. Park, J. Huh, *Macromol Res*, 2009, **17**, 181.
264. F. Brochard-Wyart, P. Martin and C. Redon, *Langmuir*, 1993, **9**, 3682.
265. P. Martin, A. Buguin and F. Brochard-Wyart, *Europhys. Lett*. 1994, **28**, 421.
266. A. Faldi, R. J. Composto and K. I. Winey, *Langmuir*, 1996, **11**, 4855.
267. P. Lambooy, K. C. Phelan, O. Haugg and G. Krausch, *Phys. Rev. Lett*., 1996, **76**, 1110.
268. S. Qu, C. J. Clarke, Y. Liu, M. H. Rafailovich, J. Sokolov, K. C. Phelan and G. Krausch, *Macromolecules* 1997, **30**, 3640.
269. G. Krausch, *J. Phys.: Condens. Matter* 1997, **9**, 7741.
270. M. Sferrazza, M. Heppenstall-Butler, R. Cubitt, D. Bucknall, J. Webster and R.A. L. Jones, *Phys. Rev. Lett.* 1998, **81**, 5173.
271. R. A. Segalman and P. F. Green, Macromolecules, 1999, 32, 801.
272. D. Slep, J. Asselta, M. H. Rafailovich, J. Sokolov, D. A. Winesett, A. P. Smith, H. Ade and S. Anders, *Langmuir* 2000, **16**, 2369.
273. C. Wang, G. Krausch and M. Geoghegan, *Langmuir*, 2001, **17**, 6269.
274. H. Kang, S. – H. Lee, S. Kim and K. Char, *Macromolecules*, 2003, **36**, 8349.
275. S. Chattopadhyay and J. C. Meredith, *Macro Rapid Comm*., 2004, **25**, 275.
276. P. Muller-Buschbaum, O. Wunnicke, M. Stamm, Y.-C. Lin and M. Muller, *Macromolecules*, 2005, **38**, 3406.
277. R. Paul and A. R. Esker, *Langmuir*, 2006, **22**, 6734.
278. R. Paul, U. Karabiyik, M. C. Swift, J. R. Hottle and A. R. Esker, *Langmuir*, 2008, **24**, 4676.
279. C. Neto *Phys. Chem. Chem. Phys*. 2007, 9, 149.
280. J. P. de Silva, M. Geoghegan, A. M. Higgins, G. Krausch, M.-O. David and G. Reiter, *Phys. Rev. Lett*., 2007, **98**, 267802.
281. L. Xu, T. Shi and L. An, *J. Chem. Phys.* 2009, **130**, 184903.
282. L. Xu, D. Bandyopadhyay, A. Sharma and S. W. Joo, *Soft Matter*, 2011, **7**, 8056.
283. L. Xu, A. Sharma and S. W. Joo, *Macromolecules*, 2011, **44**, 9335.
284. L. Xu, A. Sharma and S. W. Joo, *J. Phys. Chem. C*, 2012, **116**, 21615.
285. S. C. Thickett, A. Harris and C. Neto, *Langmuir*, 2010, **26**, 15989.
286. A. Pototsky, M. Bestehorn, D. Merkt and U. Thiele, *Phys. Rev. E*, 2004, **70**, 025201.
287. D. Bandyopadhyay, R. Gulabani and A. Sharma, *Ind. Engg. Chem Res*., 2005, **44**, 1259.

288. D. Bandyopadhyay and A. Sharma, *J. Phys. Chem*. B 2008, **112**, 11564.
289. S. Roy, D. Biswas, N. Salunke, A. Das, P. Vutukuri, R. Singh and R. Mukherjee, *Macromolecules*, 2013, **46**, 935.
290. D. Bandyopadhyay, A. Sharma and C. Rastogi, *Langmuir*, 2008, **24**, 14048.
291. D. Bandyopadhyay and A. Sharma, *J Phys. Chem. C*, 2010, **114**, 2237.
292. D. U. Ahn, Z. Wang, R. Yang and Yifu Ding, *Soft Matter*, 2010, **6**, 4900.
293. Z. Zhang, D. U. Ahn and Y. Ding, *Macromolecules*, 2012, **45**, 1972.
294. Z. Zhang, L. Wang and Y. Ding, *Langmuir*, 2013, **29**, 3073.
295. D. U. Ahn and Y. Ding, *Soft Matter*, 2011, **7**, 3794.
296. B. Z. Newby, M.K. Chaudhury and H. R. Brown, *Science*, 1995, **269**, 1407.
297. M. F. Vallat and M. Nardin, J. Adhes. 1996, **57**, 115.
298. R. J. Fields and M. F. Ashby, *Philos. Mag.*, 1976, **33**, 33.
299. Y. Urahama, J. Adhes. 1989, **31**, 47.
300. R. J. Asaro and W. A. Tiller, *Metall. Trans.*, 1972, **3**, 1789.
301. J. C. Ramirez, *Int. J. Solids Struct.*, 1989, **25**, 579.
302. P. G. Saffman and G. I. Taylor, *Proc. R. Soc. London*, Ser. A, 1958, **245**, 312.
303. V. Shenoy and A. Sharma, *Phys. Rev. Lett.*, 2001, **86**, 119.
304. V. Shenoy and A. Sharma, *J. Mech. Phys. Solids*, 2002, **50**, 1155.
305. V. Shenoy and A. Sharma, *J. Appl. Phys.*, 2003, **94**, 6376.
306. J. Sarkar, V. Shenoy and A. Sharma, *Phys. Rev. Lett.*, 2004, **93**, 018302.
307. J. Sarkar, A. Sharma and V. Shenoy, *Langmuir*, 2005, **21**, 1457.
308. J. Sarkar, A. Sharma and V. Shenoy, *J. Adhes.*, 2005, **81**, 271.
309. S. –Q. Huang, Q. –Y. Li, X. –Q. Feng , S. –W. Yu, *Mech. Mater.*, 2006, **38**, 88.
310. J. Sarkar and A. Sharma, *Langmuir*, 2010, **26**, 8464.
311. M. Gonuguntla, A. Sharma, J. Sarkar, S. A. Subramanian, M. Ghosh and V. Shenoy, *Phys. Rev. Lett.*, 2006, **97**, 018303.
312. T. Mullin, S. Deschanel, K. Bertoldi and M. C. Boyce, *Phys. Rev. Lett.*, 2007, **99**, 084301.
313. E. A. Matsumoto and R. D. Kamien, *Phys. Rev E*, 2009, **80**, 021604.
314. K. R. Shull, C. M. Flanigan, A. J. Crosby, *Phys. Rev. Lett.*, 2000, **84**, 3057.
315. A. J. Crosby, K. R. Shull, H. Lakrout and C. Creton, *J. Appl. Phys.*, 2000, **88**, 2956.
316. C. Creton and H. Lakrout, *J. Polym. Sci., Part B: Polym. Phys.*, 2000, **38**, 965.
317. C. Creton, J. Hooker, and K. R. Shull, *Langmuir*, 2001, **17**, 4948.
318. F. Yang and J. C. M. Li, *Langmuir*, 2001, **17**, 6524.
319. R. E. Webber, K. R. Shull, A. Roos and C. Creton, *Phys. Rev E*, 2003, **68**, 021805.
320. D. Derks, A. Lindner, C. Creton and D. Bonn, *J. Appl. Phys.*, 2003, **93**, 1557.
321. A. Chiche, J. Dollhofer, and C. Creton, *Eur. Phys. J. E*, 2005, **17**, 389.
322. A. Ghatak, V. Shenoy, M. K. Chaudhury and A. Sharma, *Phys. Rev. Lett.*, 2000, **85**, 4329.

323. A. Ghatak and M. K. Chaudhury, *Langmuir*, 2003, **19**, 2621.
324. A. Ghatak, L. Mahadevan and M. K. Chaudhury, *Langmuir*, 2005, **21**, 1277.
325. A. Ghatak, L. Mahadevan, J. Y. Chung, M. K. Chaudhury and V. Shenoy, *Proc. R. Soc. Lond. A*, 2004, **460**, 2725.
326. J. Y. Chung and M. K. Chaudhury, *J. R. Soc. Interface,* 2005, **2**, 55.
327. A. Ghatak, *Phys. Rev. E*, 2006, **73**, 041601.
328. A. Ghatak and M. K. Chaudhury, *J. Adhes*., 2007, **83**, 679.
329. A. Majumder, A. Ghatak and A. Sharma, *Science*, 2007, **318**, 258.
330. W. Monch and S. Herminghaus, *Europhys. Lett*. 2001, **53**, 525.
331. M. Gonuguntla, A. Sharma, R. Mukherjee and S. A. Subramanian, *Langmuir*, 2006, **22**, 7066.
332. A. Sharma, M. Gonoguntla, R. Mukherjee, S. A. Subramanian and R. Pangule, *J. Nanosci Nanotechnol*., 2007, **7**, 1744.
333. M. Gonuguntla, A. Sharma and S. A. Subramanian, *Macromolecules*, 2006, **39**, 3365.
334. R. Mukherjee, A. Sharma, M. Gonuguntla and G. K. Patil, *J. Nanosci Nanotechnol*., 2008, **8**, 3406.
335. R. Mukherjee, R. Pangule, A. Sharma and G. Tomar, *Adv. Funct. Mater.,* 2007, **17**, 2356.
336. J. Yoon, C. Q. Ru and A. A. Mioduchowski, *J. Appl. Phys*., 2005, **98**, 113503.
337. G. Tomar, A. Sharma, V. Shenoy and G. Biswas, *Phys. Rev. E.*, 2007, **76**, 011607.
338. C. Q. Ru, *J. Appl. Phys*., 2001, **90**, 6098.
339. V. Shenoy and A. Sharma, *Langmuir*, 2002**, 18***,* 2216.
340. J. Sarkar, V. Shenoy and A. Sharma, *Phys. Rev. E,* 2003, **67**, 031607.
341. J. Y. Chung, K. H. Kim, M. K. Chaudhury, J. Sarkar and A. Sharma, *Eur. Phys. J. E,* 2006, **20**, 47.
342. R. C. Pangule, I. Banerjee and A. Sharma, *J. Chem. Phys.* **128**, 154909, 2008.
343. R. Mukherjee, R. C. Pangule, A. Sharma and I. Banerjee, *J. Chem. Phys.*, 2007, **127**, 064703.
344. J. Sarkar, H. Annepu and A. Sharma, *J. Adhes.*, 2011, **87***,* 214.
345. R. Mukherjee and A. Sharma, *ACS Appl. Mater. Interfaces*, 2012, **4**, 355.
346. J. W. Swan, Proc. R. Soc. Lond. 1897, **62,** 38.
347. E. Schäffer, T. Thurn-Albrecht, T. P. Russell and U. Steiner, *Nature*, 2000, **403**, 874.
348. E. Schäffer, T. Thurn-Albrecht, T. P. Russell, and U. Steiner, *Europhys. Lett*., 2001, **53**, 518.
349. P. Deshpande, L. F. Pease III, L. Chen, S. Y. Chou and W. B. Russel, *Phys Rev E.,* 2004**, 70**, 041601.
350. K. A. Leach, Z. Lin and T. P. Russell, *Macromolecules*, 2005, **38**, 4868.
351. M. D. Dickey, E. Collister, A. Raines, P. Tsiartas, T. Holcombe, S. V. Sreenivasan, R. T. Bonnecaze and C. G. Willson, *Chem. Mater*., 2006, **18**, 2043.
352. N. E. Voicu, S. Harkema and U. Steiner, *Adv. Funct. Mater*, 2006, **16**, 926.
353. N. E. Voicu, M. S. M. Saifullah, K. R. V. Subramanian, M. E. Welland and U. Steiner, *Soft Matter*, 2007, **3**, 554.
354. P. Goldberg-Oppenheimer and U. Steiner, *Small*, 2010, **6**, 1248.

355. G. Amarandei, P. Beltrame, I. Clancy, C. O'Dwyer, A. Arshak, U. Steiner, D. Corcoran and U. Thiele, *Soft Matter*, 2012, **8**, 6333.
356. J. Heier, J. Groenewold and U. Steiner, *Soft Matter*, 2009, **5**, 3997.
357. L. F. Pease III and W. B. Russel, *J. Non-Newtonian Fluid Mech.,* 2002*,* **102**, 233.
358. L. F. Pease III and W. B. Russel, *J. Chem. Phys*., 2003, **118**, 3790.
359. N. Wu and W. B. Russel, *Appl. Phys. Lett*., 2005, **86**, 241912.
360. R. Verma, A. Sharma, K. Kargupta and J. Bhaumik, *Langmuir*, 2005, **21**, 3710.
361. S. Srivastava, P. D. S. Reddy, C. Wang, D. Bandyopadhyay and A. Sharma, *J. Chem. Phys*., 2010, **132**, 174703.
362. D. Salac, W. Lu, C.-W. Wang and A. M. Sastry, *Appl. Phys. Lett*., 2004, **85**, 1161.
363. Z. Lin, T. Kerle, M. Baker, D. A. Hoagland, E. Schäffer, U. Steiner and T. P. Russell, *J. Chem. Phys*., 2001, **114**, 2377.
364. Z. Lin, T. Kerle, T. P. Russell, E. Schäffer and U. Steiner, *Macromolecules,* 2002, **35**, 3971.
365. Z. Lin, T. Kerle, T. P. Russell, E. Schäffer and U. Steiner, *Macromolecules,* 2002, **35**, 6255.
366. M. D. Morariu, N. E. Voicu, E. Schäffer, Z. Lin, T. P. Russell and U. Steiner, *Nat. Mater*., 2003, **2**, 48.
367. M. D. Dickey, S. Gupta, K. A. Leach, E. Collister, C. G. Willson and T. P. Russel, *Langmuir*, 2006, **22**, 4315.
368. K. A. Leach, S. Gupta, M. D. Dickey, C. G. Willson, and T. P. Russell, *Chaos*, 2005, **15**, 047506.
369. V. Shankar and A. Sharma, *J. Coll. Interf. Sci*., 2004, **274**, 294.
370. R. V. Craster and O. K. Marter, *Phys. Fluids*, 2005, **17**, 032104.
371. N. Wu, M. E. Kavousanakis and W. B. Russel, *Phys. Rev. E*, 2010, **81**, 026306.
372. D. Bandyopadhyay and A. Sharma, *J. Coll. Interf. Sci.*, 2007, **311**, 595.
373. G. Tomar, V. Shankar, A. Sharma and G. Biswas, *J. Non-Newtonian Fluid Mech.,* 2007, **143**, 120.
374. D. Bandyopadhyay, A. Sharma and V. Shankar, *Euro. Phys. Lett.,* 2010, **89**, 36002.
375. D. Bandyopadhyay, A. Sharma, U. Thiele, and P. D S Reddy, Langmuir, 2009, **25**, 9108.
376. P. D. S. Reddy, D. Bandyopadhyay and A. Sharma, *J. Phys. Chem. C,* 2010, **114***,* 21020.
377. N. Arun, A. Sharma, V. B. Shenoy, and K. S. Narayan, Adv. Mater. **2006**, 18, 660.
378. N. Arun, J. Sarkar, A. Sharma, V. B. Shenoy and K. S. Narayan, *J. Adhes*., 2007**, 83,** 513.
379. J. Sarkar, A. Sharma and V. B. Shenoy, *Phys. Rev E*., 2008, **77**, 031604.
380. N. Arun, A. Sharma, P. S. G. Pattader, I. Banerjee, H. M. Dixit and K. S. Narayan, *Phys. Rev. Lett.*, 2009, **102**, 254502.
381. P. S. G. Pattader, I. Banerjee , A. Sharma and D. Bandyopadhy, *Adv. Funct. Mater*., 2011, **21**, 324.
382. E. Schäffer, S. Harkema, M. Roerdink, R. Blossey and U. Steiner, *Adv. Mater.*, 2003, **15**, 514.
383. E. Schäffer, S. Harkema, M. Roerdink, R. Blossey and U. Steiner, *Macromolecules*, 2003, **36**, 1645.
384. S. Harkema, E. Schäffer, M. D. Morariu, and U. Steiner, Langmuir, 2003, **19**, 9714.
385. R. Verma, A. Sharma, I. Banerjee and K, Kargupta, *J. Colloid Interf. Sci*., 2006, **296**, 220.
386. E. Schäffer, S. Harkema, R. Blossey and U. Steiner, *Europhys. Lett*., 2002, **60**, 255.

387. J. Peng, H. Wang, B. Li and Y. Han, *Polymer*, 2004, **45**, 8013.
388. J. Peng, R. Xing, Y. Wu, B. Li, Y. Han, W. Knoll and D. H. Kim, *Langmuir* 2007**, 23***,* 2326.
389. M. Dietzel and S. M. Troian, *Phys. Rev. Lett*., 2009, **103**, 074501.
390. S. Y. Chou, L. Zhuang and L. Guo, *Appl. Phys. Lett*. 1999, **75**, 1004.
391. S. Y. Chou and L. Zhuang, *J. Vac. Sci. Technol B*, 1999, **17**, 3197.
392. P. Deshpande, X. Sun and S. Y. Chou, *Appl. Phys. Lett*., 2001, **79**, 1688.
393. P. Deshpande and S. Y. Chou, *J. Vac. Sci. Technol. B*, 2001, **19**, 2741.
394. X. Lei, L. Wu, P. Deshpande, Z. Yu, W. Wu, H. Ge and S. Y. Chou, *Nanotechnology*, 2003, **14**, 786.
395. C. Lei, L. Zhuang, P. Deshpande and S. Y. Chou, *Langmuir*, 2005, **21**, 818.
396. J. R. Melcher, "Field-coupled surface waves", MIT Press, Cambridge, Mass. 1963.
397. L. Das, R. Mukherjee, V. Katiyar, M. Kulkarni, A. Ghatak and A. Sharma, *Adv. Mater*. 2007, **19**, 1943.
398. M. H. Lee, M. D. Huntington, W. Zhou, J. − C Yang,.; T. W. Odom, *Nano Lett*. 2011, **11**, 311.
399. N. Bhandaru, S. Roy, Suruchi, G. Harikrishnan, and R. Mukherjee, *ACS Macro Lett.* 2013, **2**, 195.

TOC Graphic Image

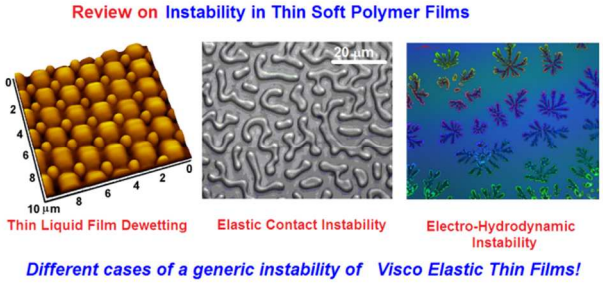

Short Biography of the Authors

Rabibrata Mukherjee is currently an Associate Professor of Chemical Engineering at the Indian Institute of Technology (IIT) Kharagpur. Rabibrata received his PhD from IIT Kanpur (2007, under the supervision of Professor Ashutosh Sharma), M. Tech IIT Kharagpur (2003) and B. E from Jadavpur University (1994). He joined IIT, Kharagpur as an Assistant Professor in the Chemical Engineering Department in 2009 and became an Associate Professor in 2013. Earlier, Rabibrata was as a Research Scientist at Central Glass & Ceramic Research Institute, Kolkata, India between 1997 and 2009. Rabibrata's research interests are soft nano patterning, thin film instability and dewetting, dewetting suppression, droplet rolling, coffee stain effect, colloidal self-assembly, electro hydrodynamic instability, etc.

Ashutosh Sharma is a Chair Professor in Chemical Engineering at the Indian Institute of Technology at Kanpur. Ashutosh received his PhD from the State University of New York at Buffalo (1987), his MS from the Pennsylvania State University (1984). He joined IIT, Kanpur as an Assistant Professor in Chemical Engineering in 1990, becoming full Professor in 1997. Ashutosh's research interests are in soft functional interfaces, micro/nano-mechanics of confined soft matter, self-organized patterning, soft nanofabrication, colloid and interfacial engineering, carbon nanocomposites and carbon MEMS/NEMS in energy, health and environmental applications, and membranes. Since January 2015 he has taken over as the Secretary to the Govt. of India, Department of Science and Technology.